Moving load in an ice channel with a crack

L. D. Zeng[a], A. A. Korobkin[b,*], B. Y. Ni[a], Y. Z. Xue[a]

[a] *College of Shipbuilding Engineering, Harbin Engineering University, Harbin 150001, China*
[b] *School of Mathematics, University of East Anglia, Norwich NR4 7TJ, United Kingdom*

Abstract

The effect of a crack in the ice cover of a channel on strains and deflections of the ice sheet, which are caused by a load moving along the channel, is investigated. The crack is at the center of the channel. The problem is symmetric with a load moving along the crack at constant speed. The problem is formulated within the linear hydroelastic theory. The fluid in the channel is inviscid and incompressible and its motion is potential. The ice sheets are modeled as viscoelastic thin plates clamped to the walls of the channel. The coupled hydroelastic problem is solved by using the Fourier transform along the channel and the normal mode method across the channel. The effects of the load speeds, depth of the channel, ice thickness and characteristics of the load on the hydroelastic response of the ice sheet are investigated. It is shown that the deflections and strains in the ice sheet strongly depend on the speed of the load with respect to the critical speeds of the hydroelastic waves propagating along the channel. The maximum ice deflection occurs at the critical speed of long waves for relatively large values of the retardation time of ice, and at the critical speed of the lowest hydroelastic wave with minimum phase speed for small retardation time of ice. The strain along the center plane of the channel peaks at the critical speed of long waves for ice sheet without a crack. However, it peaks near the critical speed of the lowest hydroelastic wave with minimum phase speed for ice sheet with a crack. The moving load causes larger strains in the ice cover if the load is elongated along the channel for a given total load and load length. The moving load causes smaller strains in the ice cover if the load is elongated along the channel for a given total load and load width.

Keywords: Moving load, ice channel, crack, ice deflections and strains

1. Introduction

One of a typical ice-water-structure interaction is that of a vehicle moving in ice covered regions. The ice cover can be used to create a road. For safe transportation on ice, it is necessary to estimate bearing capacity of the ice for a certain weight of the load moving at a certain speed along the ice. On the other hand, a moving load, such as air cushion vehicle (ACV), can be used to break the ice in order to facilitate water traffic and prevent flooding in rivers or channels. The hydroelastic responses of ice caused by moving loads are affected by presence of vertical walls and cracks in the ice. To understand and estimate the effects of vertical walls and cracks on ice response to a moving load, a linear problem of hydroelasticity is formulated and investigated in this paper for an ice channel with a crack in the ice cover along the channel. We restrict ourselves to symmetric problem, where the crack is at the center of the channel and a symmetric load moves along the crack at a constant speed.

The problem of a load moving along a floating infinite ice sheet was well studied by using the linear theory of hydroelasticity (see an excellent review in [1]). This problem starts from the pioneering work by Kheisin [2]. It is well known that there exists a critical speed for a load moving along a floating infinite elastic ice sheet. This critical speed is equal to the minimum of the phase speed of uni-directional flexural-gravity waves propagating in the ice sheet, see Davys et al. [3]. The unbounded ice response is predicted for a load moving at the critical speed on an elastic ice sheet within the linear theory of hydroelasticity. At the wavenumber, for which the minimum phase speed is achieved, the phase speed and group speed are equal. This provides a physical explanation of the unbounded response of a floating

*corresponding author: a.korobkin@uea.ac.uk

elastic ice sheet within the linear theory of hydroelasticity. In order to estimate the ice response to a load moving at the critical speed, either non linear effects (Parau and Dias [4], Bonnefoy et al. [5], Dinvay et al. [6]) or viscous damping (Hosking et al. [7], Kozin and Pogorelova [8]), or both are included in the hydroelastic model (Parau and Vanden-Broeck [9]). In present study, non linear effects are not taken into account, but the Kelvin-Voigt model of viscoelastic ice is used to estimate the finite ice response at the critical speeds.

Tabata [10] investigated the viscoelastic properties of the sea ice by performing experiments with rectangular floating ice beams under given static loads. The curves for bending stresses in the ice beams as functions of time were obtained. By analysing the measured stresses Tabata concluded that "viscoelastic properties of sea ice are analogous to a rheological model of Maxwell unit and a Voigt (Kelvin) unit connected in series. Therefore, viscoelastic properties of sea ice can be expressed by four characteristic constants." Takizawa [11] conducted systematic field experiments with a vehicle moving on the ice sheet by measuring the deflections of the ice sheet. He found that the position of the maximum ice deflection lagged behind the vehicle, even for a fairly low speed. Then the lag time as a function of the vehicle speed was determined. By assuming the lag time equal to the retardation time of ice, the viscosity of ice was evaluated. In addition, Takizawa [11] determined the critical speed for the ice sheet, for which the deflection of the ice sheet was maximum. The maximum ice deflection for a moving load was three times higher than the maximum deflections under an equivalent static load. Hosking et al. [7] used a two-parameter viscoelastic model of ice to study the response of a floating infinite ice sheet to a moving vehicle. Viscoelastic models of ice provide finite ice response at the critical speed of infinite elastic ice sheet and explain exponential decay of waves generated by the moving load with the distance from the load. Kozin and Pogorelova [8] used the Kelvin-Voigt model, Maxwell model and generalized Maxwell-Kelvin models to describe viscoelastic characteristics of ice and compared their theoretical predictions of ice response within these three models with the experimental results by Takizawa [11]. They concluded that the retardation time, which represents the viscosity of ice, should be a function of the load speed in these three models to obtain reasonable results.

Cracks can exist in the ice sheet. In a mathematical model, a crack is of zero width and completely separates the ice sheets. Diffraction of hydroelastic waves propagating in an ice sheet with cracks was fairly well studied. Such as waves propagating in an ice sheet with a single straight-line crack (Evans and Porter [12]), with multiple straight-line cracks parallel to each other (Porter and Evans [13]), and with multiple cracks of arbitrary shapes (Li et al. [14]). Williams and Porter [15] studied waves propagating through two semi-infinite elastic ice sheets of different thickness separated by a crack. They found that edge waves exist in the presence of the crack and for plates of different thicknesses, however, the difference between the thicknesses must be small. Tkacheva [16] studied the problem of a load moving on infinite elastic ice sheet with a crack by using the Wiener-Hopf technique within the linear hydroelasticity theory. The thicknesses of the two semi-infinite ice sheets were different. It was shown that the edge wave modes are excited only if the two ice sheets are of the same thickness and the load is moving at a supercritical speed. Xue et al. [17] considered a load moving on an infinite ice sheet with a crack by using a boundary element method. The Kelvin-Voigt model of viscoelastic ice was used. It was shown that the presence of a crack made the ice sheet easier to deform but more difficult to break comparing with the results for the equivalent infinite ice sheet without a crack. The load speed providing the maximum ice deflection and stress was found to be larger than the critical speed for the equivalent infinite elastic ice sheet, due to the combined effects of boundary conditions and damping of the ice sheet.

The problem of a load moving along an ice-covered channel, such as rivers and channels, also received considerable attention. Differently from an infinite elastic ice sheet with just two critical speeds, there are infinitely many hydroelastic waves with their own critical speeds for a channel fully covered by elastic ice sheet (Korobkin et al. [18], Batyaev and Khabakhpasheva [19], Ren et al. [20]). Korobkin et al. [18] considered the problem of waves propagating along a frozen channel with elastic ice sheet clamped to the walls of the channel. Batyaev and Khabakhpasheva [19] studied similar problem but with free edge conditions between the ice sheet and channel walls. Ren et al. [20] studied this problem for various edge conditions between the ice sheet and channel walls. The dispersion relations and critical speeds of hydroelastic waves in a frozen channel are helpful to understand the ice response to a load moving along the frozen channel. By using these results, Shishmarev et al. [21] studied the problem of a load moving along a frozen channel with a constant speed using the Fourier transform along the channel and the normal mode method across the channel. Kelvin-Voigt model of ice was used. The ice sheet was clamped to the channel walls. The steady state solution of the problem in the coordinate system moving together with the load was obtained and studied numerically. It was shown that the deflection and strain in the ice sheet quickly decay with the distance from the load due to the viscoelastic properties of the ice. The rate of decay is related to the retardation time, which can be estimated using field

measurements. The presence of the walls decreases the ice deflections but increases the strains in comparison with the results for the ice sheet of infinite extent. The speed of the load strongly affects the ice response. The critical speed was found in term of the maximum deflection, which is larger than the minimum phase speed of the first hydroelastic wave, in Korobkin et al. [18]. The maximum strain is achieved under the load for the load speed smaller than the minimum phase speed of the first hydroelastic wave, but on the walls for the load speed greater than the minimum phase speed of the first hydroelastic wave. Khabakhpasheva et al. [22] studied the time-dependent problem of a load moving along a frozen channel without viscosity effects to be considered in the ice model. The load was starting its motion from the rest and then moving with a constant speed. It was shown that the large-time deflection of the ice sheet consists of steady deflection and standing waves in front and behind the load in the coordinate system moving together with the load.

In the present work, we focus on a load moving along an ice-covered channel with a crack in the center plane of the channel. The crack is of zero width. The Kelvin-Voigt model of viscoelastic ice is used. The ice sheets on both sides of the crack are clamped to the walls of the channel. The load is symmetric about the center line of the ice channel. The deflection and stain in the ice sheet are stationary in the coordinate system moving together with the load.

The paper is organized as follows. The formulation of the problem is given in Section 2. The Fourier transform along the channel and the normal mode method across the channel are used to solve the problem in Section 3. Numerical algorithms and results are presented in Section 4. Conclusions are drawn and future work is discussed in Section 5.

2. Formulation of the problem

The problem of a load moving at a constant speed U along an ice channel with a crack in the ice cover is considered, see figure 1. A coordinate system moving together with the external load along the channel is used. The origin O of the system is located at the center plane of the channel. The z-axis points upwards, opposite to the gravitational acceleration $\vec{g}$. The x-axis points to the longitudinal direction of the channel and is perpendicular to the plane of figure 1. The channel is of rectangular cross section with constant depth H and width $2L$. The channel is of infinite extent in the x-direction. The channel is occupied with liquid of density ρ. The liquid is inviscid and incompressible. The ice sheet is modeled by thin viscoelastic plate [23]. The ice sheet is of constant thickness h and with rigidity $D = Eh^3/[12(1-\nu^2)]$, where E is Young's modulus of ice and ν is Poisson's ratio. The ice sheet floats on the water surface, is frozen to the vertical walls of the channel, and is divided into two pieces by a crack at $y = 0$. The moving external load is modeled by a given pressure $P(x, y)$ acting over the upper surface of the ice sheet. We assume that both the ice deflection and the flow under the ice are stationary in the moving coordinate system.

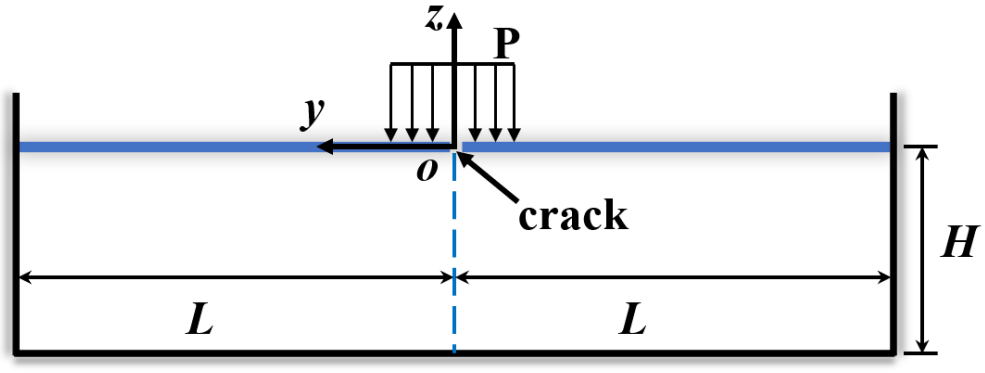

Figure 1: Sketch of a load moving along a channel covered by ice sheet with a crack in the middle of the sheet.

The deflection of the ice sheet, $z = w(x, y)$, is a solution of the viscoelastic plate equation written in the moving coordinates (Shishmarev et al. [21] and Mase [23]),

$$D(1-\tau U\frac{\partial}{\partial x})\nabla^4 w + mU^2\frac{\partial^2 w}{\partial x^2} = p(x,y,0) - P(x,y) \quad (-L < y < L, -\infty < x < \infty, z = 0), \tag{1}$$

where $\tau = \eta/E$ is the retardation time, η is the viscosity of the ice, $\nabla^4 = \partial^4/\partial x^4 + 2\partial^4/(\partial x^2 \partial y^2) + \partial^4/\partial y^4$ is the biharmonic operator, $m = \rho_i h$ is the mass of the ice plate per unit area, ρ_i is the ice density, $p(x, y, 0)$ is the hydrodynamic pressure acting on the lower surface of the ice sheet, $P(x, y)$ is the external pressure. The external pressure $P(x, y)$ is taken to be a positive constant P_0 in the region $|x| < a$ and $|y| < b$ and zero otherwise,

$$P(x, y) = P_0(\mathcal{H}(x + a) - \mathcal{H}(x - a))(\mathcal{H}(y + b) - \mathcal{H}(y - b)), \tag{2}$$

where a and b are positive constants and $\mathcal{H}(x)$ is the Heaviside function, which is equal to zero for negative and one for positive x. We restrict ourselves here to symmetric loads, however, the analysis can be readily extended to loads moving closer to one of the walls and with more complex distributions. Then, the deflection of the ice sheets across the channel is also symmetric, $w(x, -y) = w(x, y)$. The crack at $y = 0$ separates the ice sheets with zero gap between them. The ice sheet deflection is not continuously differentiable at $y = 0$, where the ice edges are free of stresses and shear forces,

$$\left(\frac{\partial^2}{\partial y^2} + \nu\frac{\partial^2}{\partial x^2}\right) w = 0, \qquad \frac{\partial}{\partial y}\left(\frac{\partial^2}{\partial y^2} + (2 - \nu)\frac{\partial^2}{\partial x^2}\right) w = 0 \quad (y = \pm 0, -\infty < x < \infty). \tag{3}$$

The other edges of the ice sheets are frozen to the vertical walls of the channel,

$$w = 0, \qquad \frac{\partial w}{\partial y} = 0 \qquad (y = \pm L, -\infty < x < \infty). \tag{4}$$

The hydrodynamic pressure $p(x, y, 0)$ acting on the ice/water interface is given in the moving coordinate system by the linearized Bernoulli equation,

$$p(x, y, 0) = \rho U\frac{\partial \varphi}{\partial x} - \rho g w \quad (-\infty < x < \infty, -L < y < L), \tag{5}$$

where $\varphi(x, y, z)$ is the velocity potential of the flow beneath the ice sheet, which satisfies the Laplace equation in the flow region,

$$\varphi_{xx} + \varphi_{yy} + \varphi_{zz} = 0 \qquad (-\infty < x < \infty, -L < y < L, -H < z < 0), \tag{6}$$

and the boundary conditions,

$$\frac{\partial \varphi}{\partial y} = 0 \qquad (y = \pm L), \qquad \frac{\partial \varphi}{\partial z} = 0 \qquad (z = -H), \qquad \frac{\partial \varphi}{\partial z} = -U\frac{\partial w}{\partial x} \qquad (z = 0), \tag{7}$$

where the third equation is the linearized kinematic boundary condition. Due to the viscoelastic properties of the ice sheet, the disturbances caused by the moving load decay with the distance from the load,

$$w, \varphi \to 0 \qquad (|x| \to \infty). \tag{8}$$

The formulated problem is considered in dimensionless variables denoted by tilde. The half-width of the channel L is taken as the length scale, the ratio $\sqrt{L/g}$ as the time scale, and the pressure magnitude P_0 as the pressure scale. Then, $\tilde{x} = x/L$, $\tilde{y} = y/L$, $\tilde{z} = z/L$, $\tilde{H} = H/L$, $\tilde{h} = h/L$, $\tilde{\tau} = \tau/\sqrt{L/g}$, $\tilde{a} = a/L$, $\tilde{b} = b/L$, and $\tilde{P} = P/P_0$. We denote $\tilde{w} = w/w_{sc}$ and $\tilde{\varphi} = \varphi/\varphi_{sc}$, where $w_{sc} = P_0/(\rho g)$ and $\varphi_{sc} = P_0\sqrt{L/g}/\rho$ are chosen as the scales of ice deflection and the velocity potential correspondingly. The characteristic length of the ice sheet is defined as $L_c = (D/\rho g)^{1/4}$ and can be used to estimate whether the presence of the side walls of the channel is important for ice response as was studied by Shishmarev et al. [21].

In the dimensionless variables, the formulated problem reads (tildes are omitted below)

$$\beta(1 - \tau \mathrm{Fr}\frac{\partial}{\partial x})\nabla^4 w + \alpha \mathrm{Fr}^2 w_{xx} + w = \mathrm{Fr}^2\varphi_x - P(x, y) \quad (-\infty < x < \infty, -1 < y < 1, z = 0), \tag{9}$$

$$\varphi_{xx} + \varphi_{yy} + \varphi_{zz} = 0 \qquad (-\infty < x < \infty, -1 < y < 1, -H < z < 0), \tag{10}$$

$$\frac{\partial \varphi}{\partial y} = 0 \qquad (y = \pm 1), \qquad \frac{\partial \varphi}{\partial z} = 0 \qquad (z = -H), \qquad \frac{\partial \varphi}{\partial z} = -\frac{\partial w}{\partial x} \qquad (z = 0), \tag{11}$$

$$w = 0, \qquad \frac{\partial w}{\partial y} = 0 \qquad (y = \pm 1, -\infty < x < \infty), \tag{12}$$

$$\left(\frac{\partial^2}{\partial y^2} + \nu\frac{\partial^2}{\partial x^2}\right)w = 0, \qquad \frac{\partial}{\partial y}\left(\frac{\partial^2}{\partial y^2} + (2-\nu)\frac{\partial^2}{\partial x^2}\right)w = 0 \qquad (y = \pm 0, -\infty < x < \infty), \tag{13}$$

$$w, \varphi \to 0 \qquad (|x| \to \infty). \tag{14}$$

where $\beta = D/(\rho g L^4)$, $\alpha = \rho_i h/(\rho L)$ and $\mathrm{Fr} = U/\sqrt{gL}$ is the Froude number.

The solution of the problem (9)-(14) depends on seven dimensionless parameters β, τ, α, H, Fr, a and b. These parameters describe the characteristics of ice, cross section of the channel and the characteristics of the external load. We shall determine the ice deflection $w(x, y)$ and strain distribution in the ice sheet, and study their dependence on the dimensionless parameters with a particular focus on the Froude number. The Froude number Fr is the only parameter which involves the speed of the load U.

In the linear theory of hydroelasticity, the strains in the ice plate vary linearly through the ice thickness being zero at the middle of the plate. At any location, the maximum strain is achieved at the surface of the ice plate. We are concerned here only with positive strains which correspond to elongation of the ice surface and tensile stresses at this surface. The scale of the strain is taken as $\epsilon_{sc} = hP_0/(2\rho g L^2)$. Based on a standard definition of principal strains [24], they are equal to the eigenvalues of the strain tensor

$$\epsilon(x, y) = -\zeta\begin{pmatrix} w_{xx} & w_{xy} \\ w_{xy} & w_{yy} \end{pmatrix}, \tag{15}$$

where ζ is the dimensionless coordinate across the ice thickness, $-1 \le \zeta \le 1$. The maximum magnitude of the principal strains at a certain point of the plate provides the maximum strain at this point. The direction of the maximum strain is determined using the eigenvectors of the strain tensor. The strains are proportional to the pressure P_0 of the external load within the linear theory. The linear theory of hydroelasticity can be used when the local slope of the plate, $\sqrt{w_x^2 + w_y^2}$, is small and the strains in the ice sheet are below the yield strain ϵ_{cr} of the ice.

The yield strength of a material is defined as the strain $\epsilon = \epsilon_{cr}$ at which a material begins to deform plastically. Strains in the ice sheet should be below the yield strain, to prevent our viscoelastic ice model from being unrealistic. Strains greater than the yield strain ϵ_{cr} are expected to lead to ice fracture. In this study, the yield strain for the ice is taken as $\epsilon_{cr} = 8 \cdot 10^{-5}$ (Brocklehurst et al. [25]).

3. Solution of the problem

The coupled problem (9)-(14) is solved using the Fourier transform in the x- direction. The plate equation (9) provides

$$\beta(1 - i\xi\tau\mathrm{Fr})(w^F_{yyyy} - 2\xi^2 w^F_{yy} + \xi^4 w^F) + (1 - \alpha\mathrm{Fr}^2\xi^2)w^F = i\xi\mathrm{Fr}^2\varphi^F - P^F(\xi, y) \quad (0 < y < 1), \tag{16}$$

where

$$w^F(\xi, y) = \frac{1}{\sqrt{2\pi}}\int_{-\infty}^{\infty} w(x, y)e^{-i\xi x}\mathrm{d}x, \quad P^F(\xi, y) = \frac{1}{\sqrt{2\pi}}\int_{-\infty}^{\infty} P(x, y)e^{-i\xi x}\mathrm{d}x.$$

Since $w(x, y)$ is an even function of y, so is $w^F(\xi, y)$. The normal mode method, see for example Korobkin et al. [18] provides that the solution, $w^F(\xi, y)$, can be sought as the following superposition,

$$w^F(\xi, y) = \sum_{n=1}^{\infty} F_n(\xi)\psi_n(|y|) \qquad (0 < |y| < 1), \tag{17}$$

of the elastic modes $\psi_n(y)$ with their coefficients $F_n(\xi)$ to be determined. The modes $\psi_n(y)$ are non-trivial solutions of the eigenvalue problem,

$$\left.\begin{gathered}\left(\frac{\mathrm{d}^2}{\mathrm{d}y^2}-\xi^2\right)^2\psi_n=\lambda_n^4\psi_n\quad(0<y<1),\\ \psi_n''(0)=\nu\xi^2\psi_n(0),\quad \psi_n'''(0)=(2-\nu)\xi^2\psi_n'(0),\\ \psi_n(1)=0,\quad \psi_n'(1)=0,\end{gathered}\right\}\tag{18}$$

with the corresponding eigenvalues λ_n. The modes $\psi_n(y)$ are given by Zeng et al. [26]

$$\psi_n(y)=A_n\left[\frac{\sin(q(y-1))}{q}-\frac{\sinh(p(y-1))}{p}+Q(\lambda_n)\cos(q(y-1))-Q(\lambda_n)\cosh(p(y-1))\right],\tag{19}$$

where $p=\sqrt{\lambda_n^2+\xi^2}$, $q=\sqrt{\lambda_n^2-\xi^2}$, and

$$Q(\lambda_n)=\frac{[\lambda_n^2+(1-\nu)\xi^2]\frac{\sinh(p)}{p}+[\lambda_n^2-(1-\nu)\xi^2]\frac{\sin(q)}{q}}{[\lambda_n^2+(1-\nu)\xi^2]\cosh(p)+[\lambda_n^2-(1-\nu)\xi^2]\cos(q)}.$$

The eigenvalues λ_n are the solutions of the equation

$$\frac{\lambda_n^4-(1-\nu)^2\xi^4}{\lambda_n^4+(1-\nu)^2\xi^4}+\cosh(p)\cos(q)=\left[\xi^2-\frac{2\lambda_n^4(1-\nu)\xi^2}{\lambda_n^4+(1-\nu)^2\xi^4}\right]\frac{\sinh(p)}{p}\frac{\sin(q)}{q},$$

where λ_n are real with $\lambda_{n+1}>\lambda_n$ and $n\geq 1$. The coefficients A_n in (19) are such that the modes $\psi_n(y)$ are orthonormal,

$$\int_0^1\psi_n(y)\psi_m(y)\mathrm{d}y=\delta_{nm},\tag{20}$$

where $\delta_{nn}=1$ and $\delta_{nm}=0$ for $n\neq m$. Note that the modes $\psi_n(y)$ and the eigenvalues λ_n depend on the parameter of the Fourier transform ξ.

Substituting (17) and (18) into (16), one finds

$$\sum_{n=1}^{\infty}F_n(\xi)\left[\beta\lambda_n^4(1-i\xi\tau\mathrm{Fr})+1-\alpha\mathrm{Fr}^2\xi^2\right]\psi_n(y)=i\xi\mathrm{Fr}^2\varphi^F-P^F(\xi,y)\quad(0<y<1).\tag{21}$$

The kinematic condition at the ice-liquid interface, the third condition in (11), provides that $\varphi^F(y,z,\xi)$ can be presented as

$$\varphi^F(y,z,\xi)=-i\xi\sum_{n=1}^{\infty}F_n(\xi)\Phi_n(y,z,\xi),\tag{22}$$

where the potentials Φ_n, $n\geq 1$, are the solutions of the following boundary value problems,

$$\Phi_{n,yy}+\Phi_{n,zz}=\xi^2\Phi_n\qquad(|y|<1,-H<z<0),\tag{23}$$

$$\Phi_{n,y}=0\quad(y=\pm1),\qquad\Phi_{n,z}=0\quad(z=-H),\qquad\Phi_{n,z}=\psi_n(|y|)\quad(z=0).\tag{24}$$

Multiplying both sides of (21) by $\psi_k(y)$, integrating the result in y from 0 to 1, and using relation (20) and equation (22), we find

$$F_k(\xi)\left[\beta\lambda_k^4(1-i\xi\tau\mathrm{Fr})+1-\alpha\mathrm{Fr}^2\xi^2\right]-\xi^2\mathrm{Fr}^2\sum_{n=1}^{\infty}F_n(\xi)C_{kn}=-P_k,\tag{25}$$

where

$$C_{kn}(\xi)=\int_0^1\Phi_n(y,0,\xi)\psi_k(y)\mathrm{d}y,\qquad P_k(\xi)=\int_0^1P^F(\xi,y)\psi_k(y)\mathrm{d}y.$$

The system (25) can be written in the matrix form,

$$\begin{gathered}\mathbf{A}\vec{F} = \vec{P},\\ \mathbf{A} = \mathrm{Fr}^2\xi^2\mathbf{C} - \beta(1 - i\xi\tau\mathrm{Fr})\mathbf{B} + (\alpha\mathrm{Fr}^2\xi^2 - 1)\mathbf{I},\end{gathered} \tag{26}$$

where $\vec{F} = (F_1, F_2, F_3, ...)^T$, $\vec{P} = (P_1, P_2, P_3, ...)^T$, $\mathbf{I}$ is the unit matrix, $\mathbf{B}$ is the diagonal matrix with elements λ_n^4, and $\mathbf{C} = \{C_{kn}\}_{k,n=1}^{\infty}$. The coefficients $C_{kn}(\xi)$ are calculated analytically for each ξ in Appendix A. The asymptotic formula for the coefficients as $\xi \to 0$ is also given there. Note that the imaginary part of the matrix $\mathbf{A}$ is proportional to the dimensionless retardation time τ.

To solve equation (26) we distinguish the real and imaginary parts of the vector $\vec{F}$, $\vec{F} = \vec{F}^R + i\vec{F}^I$. Separating the real and imaginary parts in (26), we arrive at systems of nonhomogeneous equations with respect to $\vec{F}^R$ and $\vec{F}^I$ with symmetric matrices. Namely, equation (26) can be written as

$$\begin{cases}\left[\mathrm{Fr}^2\xi^2\mathbf{C} - \beta\mathbf{B} + (\alpha\mathrm{Fr}^2\xi^2 - 1)\mathbf{I}\right]\vec{F}^R - \beta\xi\tau\mathrm{Fr}\mathbf{B}\vec{F}^I = \vec{P},\\ \beta\xi\tau\mathrm{Fr}\mathbf{B}\vec{F}^R + \left[\mathrm{Fr}^2\xi^2\mathbf{C} - \beta\mathbf{B} + (\alpha\mathrm{Fr}^2\xi^2 - 1)\mathbf{I}\right]\vec{F}^I = 0.\end{cases} \tag{27}$$

In the present problem, $P_k(\xi)$ are even functions of ξ. It can be shown that $F_n^R(\xi)$ are even and $F_n^I(\xi)$ are odd functions of ξ. The deflection $w(x, y)$ is obtained by the inverse Fourier transform,

$$w(x, y) = \sqrt{\frac{2}{\pi}}\sum_{n=1}^{\infty}\psi_n(y)\int_0^{\infty}(F_n^R(\xi)\cos(\xi x) - F_n^I(\xi)\sin(\xi x))\mathrm{d}\xi \quad (0 \le y \le 1), \tag{28}$$

once the functions $F_n^R(\xi)$ and $F_n^I(\xi)$ have been determined as solutions of the system (27) for any $\xi \ge 0$. We denote the integrals in (28) by $W_n(x)$, and retain N lowest modes in the series (28) in our numerical results. The integrals $W_n(x)$ are evaluated numerically by trapezoidal rule for a finite interval which is large enough. Then equation (28) is approximated by

$$w(x, y) \approx \sqrt{\frac{2}{\pi}}\sum_{n=1}^{N}\psi_n(y)W_n(x). \tag{29}$$

Both the interval and the step of integration in $W_n(x)$, and the number of retained modes N are carefully selected to guarantee that (29) well approximates the deflection (28) for $0 \le y \le 1$ and an x-interval of interest. The second derivatives of the plate deflection in the strain tensor (15) are obtained by differentiation of the integrals in (28). The convergence test for the second derivatives has been also performed.

4. Numerical results

The results of the present study are presented in terms of the ice deflections and strains in the moving coordinate system. Calculations are performed for a freshwater ice with density $\rho_i = 917$ kg m^{-3}, Young's modulus $E = 4.2 \times 10^9$ N m^{-2} and Poisson's ratio $\nu = 0.3$. The ice thickness h is varied from 5 cm to 20 cm. The retardation time τ of the ice sheet is varied from 0.001 s to 1 s. The half-width L of the channel is 10 m and the water depth H is varied from 2 m to 10 m. Water density is $\rho = 1000$ kg m^{-3} and the gravity acceleration is $g = 9.81$ m s^{-2}. The load (2) is applied over a square area, $a = b = 1$ m, with $P_0 = 1000$ Pa. The ranges of the load speed U is chosen according to the critical speeds of hydroelastic waves propagating in the ice channel with a crack. The load speed U is varied from 3 m/s to 20 m/s in the present study.

The infinite algebraic system (26) is truncated leaving N equations and N complex unknowns. The linear system (27) of $2N$ equations is solved M times for $\xi = \xi_m$, $1 \le m \le M$ and $\xi_1 = 0$, with a step $\Delta\xi$. Note that the left hand side of the linear system (27) is not equal to zero for $\xi_1 = 0$. The elements of (27) for $\xi_1 = 0$ are given in Appendix A, see (A.7). The asymptotic solution of linear system (27) as $\xi \to 0$ is given in Appendix B.

The step, $\Delta\xi$, the length of the integration interval, ξ_M, and the number of modes, N, are carefully selected to ensure that the ice deflection (28) are evaluated with required accuracy. In terms of the convergence analysis, we found that $\xi_M = 25$, $\Delta\xi = 0.001$ and $N = 10$ provide accurate solution. If we increase the values of ξ_M and/or N by

50%, or decrease the value of $\Delta\xi$ by 50%, then the ice deflection changes less than by 0.1%. Figure 2 illustrates the effect of the length of the integration interval, ξ_M, on the ice deflections and strains for Fr = 0.716. It is seen that $\xi_M = 5$ and $\xi_M = 25$ give curves, which are graphically almost identical, with the relative difference of ice deflections and strains being less than 0.1% and 0.5%, respectively. Higher accuracy of the results can be achieved by further increasing both ξ_M and N, and decreasing $\Delta\xi$. Note that the strains depend on the second y-derivative of the ice deflection. Thus, a good accuracy of the numerical strains means good accuracy of the ice deflection, which is also clear from figure 2.

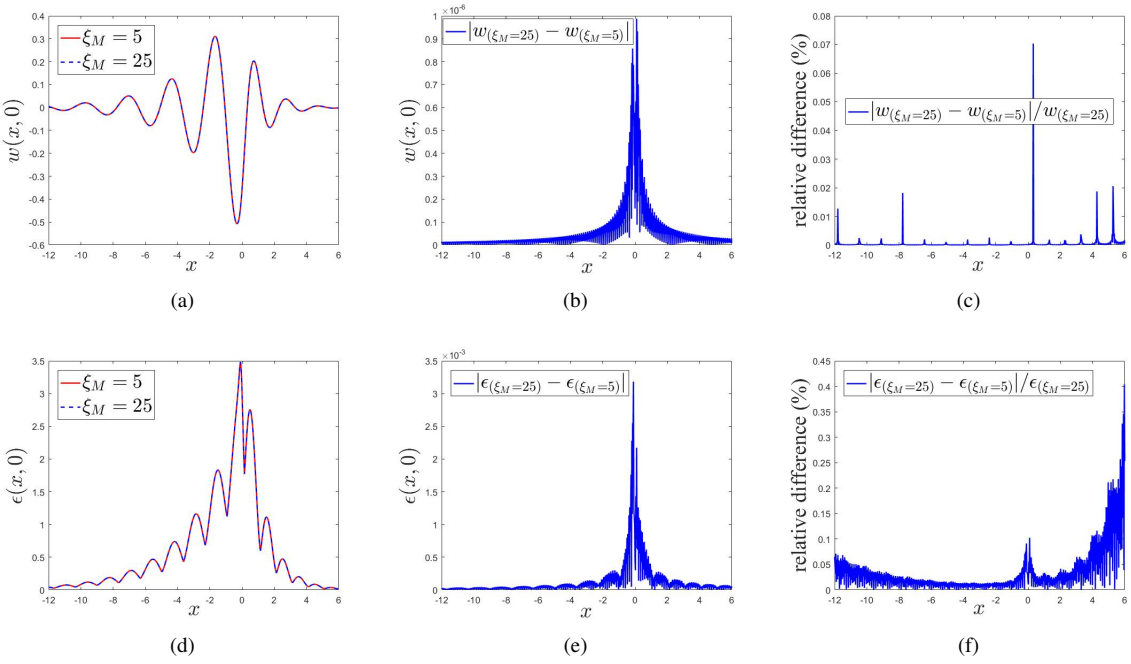

Figure 2: Convergence analysis of ice deflection (a-c) and strain (d-f) with respect to ξ_M for $H = 0.5$, $h = 0.01$, $\tau = 0.1$ s and Fr = 0.716.

The ice deflection caused by a load moving in an ice channel can be related to the hydroelastic waves propagating along the ice channel at the speed equal to the speed of the load. Note that the problem of waves propagating along the ice channel does not include any damping. It is known that the deflection of an elastic ice sheet peaks at a speed of the load equal to a so-called critical speed of a hydroelastic wave within the linear theory. The critical speed of a hydroelastic wave is the phase speed of the wave at a certain wavenumber k, where the phase speed is equal to the group speed of the wave (Shishmarev et al. [21]). The phase speeds $c^{(n)}(k) = \omega^{(n)}(k)/k$ of the waves propagating along an ice channel with a crack in the center plane of the channel were determined by Ren et al. [20] using the finite water depth model (FWD) as in the present paper, and were studied by Zeng et al. [27] using the shallow water approximation (SWA). Here k is the wave number and $\omega^{(n)}(k)$ is the corresponding wave frequency. The phase speeds of waves propagating in an ice channel without crack were studied by Korobkin et al. [18] using FWD. The hydroelastic waves propagating along the channel with the phase speed $c^{(n)}(k)$ equal to the speed of the load U are described by equations (27) without damping, $\tau = 0$, without a load, $\vec{P} = 0$, where ξ is changed to k and the Froude number Fr $= U/\sqrt{gL}$ to $c^{(n)}(k)/\sqrt{gL}$. Then the product $\mathrm{Fr}^2\xi^2$ in (27) is equal to $[\omega^{(n)}(k)]^2 L/g$. The solutions of the reduced system (27) and the series (17) provide the deflections of the hydroelastic waves in the moving coordinate system as $w_n(x, y) = F_n(y, k)\cos(kx)$. The condition of solvability of (27) gives the dispersion relations for the wave frequencies $\omega^{(n)}(k)$. In this section, we use dimensionless wave frequency $\tilde{\omega}^{(n)}(k) = \omega^{(n)}(k)/\sqrt{g/L}$, dimensionless phase speeds $\tilde{c}^{(n)}(k) = c^{(n)}(k)/\sqrt{gL}$ and dimensionless wavenumber $\tilde{k} = kL$, tildes are omitted below. The dispersion relations $\omega^{(n)}(k)$, where $n \geq 1$ and $\omega^{(n+1)}(k) > \omega^{(n)}(k)$, obtained in this way are the same as in Korobkin et al. [18] and Zeng et al. [26] for specific conditions.

The dimensionless phase speeds of the first two even hydroelastic waves as functions of the dimensionless

wavenumber are shown in figure 3 for the conditions specified above. It is seen that the phase speeds of the first mode, $c^{(1)}(k)$, for the ice channels with crack and without crack are close to other each. The phase speed at which the derivative of the phase speed is equal to zero is called the critical speed (Davys et al. [3]). The phase speed is equal to the group speed at such a critical speed. A load moving at a critical speed generates waves with the phase and group speeds equal to the speed of the load. The speed of energy propagation with these waves from the load is equal to the group speed. Therefore, the energy of both the flow and ice deflection generated by the moving load, does not propagate from the load if the load moves at the critical speed. As a result, the ice deflections increase in time with possible breaking of the ice if damping in the ice plate is not taken into account. The slope of the phase speed $c^{(1)}(k)$ at $k = 0$, see figure 3, is zero. This suggests that $\omega^{(1)}(k) \sim c^{(1)}(0)k$ for small wavenumbers k. Then the corresponding group speed, $d\omega^{(1)}(k)/dk$, at $k = 0$ is equal to the phase speed $c^{(1)}(0)$, which is the condition for this speed to be a critical speed. A critical speed of a moving load is defined as a speed at which the corresponding group and phase speeds are equal, see Kausel et al. [28]. The phase speed is the speed of the load and the speed of the waves generated by the load. In the moving coordinate system, these waves do not propagate from the load. The group speed is the speed of energy propagation from the load. If the group speed is equal to the load speed, then the energy transmitted from the load to the ice and the water does not propagate from the load accumulating near the load with time and leading to unbounded ice response when no damping is included in the ice model. This critical speed for long flexural-gravity waves is equal to $\sqrt{gH}$ for unbounded ice sheet: note that this value is independent of the elastic characteristics of the ice sheet and is the same as for gravity waves. In the present problem of an ice sheet in a channel, the critical speed $c^{(1)}_{cr,2}$ depends on the elastic properties of the ice sheet and on the channel dimensions, as well as on the presence of cracks in the ice sheet. Each wave mode in the ice channel has a single critical speed for $k > 0$. These critical speeds are denoted as $c^{(n)}_{cr,1}$. Note that some flexural-gravity waves in an ice channel with a lead of non-zero width can have several critical speeds for the same mode, see Zeng et al. [26]. Table 1 lists dimensionless critical speeds $c^{(1)}_{cr,2}$ for dimensionless water depth $H = 0.2$, 0.5 and 1, which are obtained from figure 3. The critical speeds $c^{(1)}_{cr,2}$ for unbounded ice sheet are also presented in table 1 for reference. It is seen that the critical speeds $c^{(1)}_{cr,2}$ increase with increase of the water depth. SWA predicts $c^{(1)}_{cr,2}$ very well, which is not a surprise because this critical speed is for long hydroelastic waves. This critical speed in the channel is higher than the corresponding critical speed for unbounded ice sheet. The presence of the crack makes $c^{(1)}_{cr,2}$ smaller. We also investigated the effect of the ice thickness on the critical speeds $c^{(1)}_{cr,2}$ and $c^{(1)}_{cr,1}$ for dimensionless water depth $H = 0.5$, see table 2. The critical speeds $c^{(1)}_{cr,2}$ and $c^{(1)}_{cr,1}$ listed in table 2 are obtained from figure 4. The critical speeds increase with increase of the ice thickness. The critical speed $c^{(1)}_{cr,2}$ for the ice channel with $h = 0$ is equal to the critical speed for unbounded ice sheet as expected. Table 3 provides the critical speeds $c^{(1)}_{cr,1}$ and $c^{(2)}_{cr,1}$ for dimensionless water depth $H = 0.2$, 0.5 and 1.

Table 1: The critical speeds, $c^{(1)}_{cr,2}$, for the ice channels with a crack in the center plane of the channel and without the crack, and for the unbounded ice sheet with the dimensionless ice thickness $h = 0.01$.

$c^{(1)}_{cr,2}$	crack(FWD)	crack(SWA)	no crack(FWD)	unbounded ice sheet
$H = 0.2$	0.553	0.553	0.555	0.447
$H = 0.5$	0.874	0.874	0.879	0.707
$H = 1$	1.236	1.236	1.243	1.000

The maximum and minimum of the dimensionless ice deflection, $w^{(y=0)}_{\max}(\mathrm{Fr}) = \max_{|x|<\infty}\{w(x,0)\}$ and $w^{(y=0)}_{\min}(\mathrm{Fr}) = \min_{|x|<\infty}\{w(x,0)\}$, along $y = 0$ as functions of the dimensionless load speed, Fr, are shown in figure 5 with and without a crack for dimensionless water depth $H = 0.5$. The dimensionless ice thickness is $h = 0.01$. The dimensional retardation time of the ice sheet is $\tau = 0.1$ s. For ice sheet with a crack, figure 5(a) shows that $w^{(y=0)}_{\min}(\mathrm{Fr})$ peaks at $\mathrm{Fr} = 0.873$, and $w^{(y=0)}_{\max}(\mathrm{Fr})$ peaks at $\mathrm{Fr} = 0.874$, which are close to the critical speed of long waves for ice sheet with a crack, $c^{(1)}_{cr,2}$, for $H = 0.5$, see table 1. Note that $w^{(y=0)}_{\max}(\mathrm{Fr})$ and $w^{(y=0)}_{\min}(\mathrm{Fr})$ peak locally at $\mathrm{Fr} = 0.737$ and $\mathrm{Fr} = 0.723$, respectively, which are close to the critical speed of the first hydroelastic wave, see Table 1. However, these peaks are less pronounced, which could be caused by the relatively large value of the retardation time of ice for

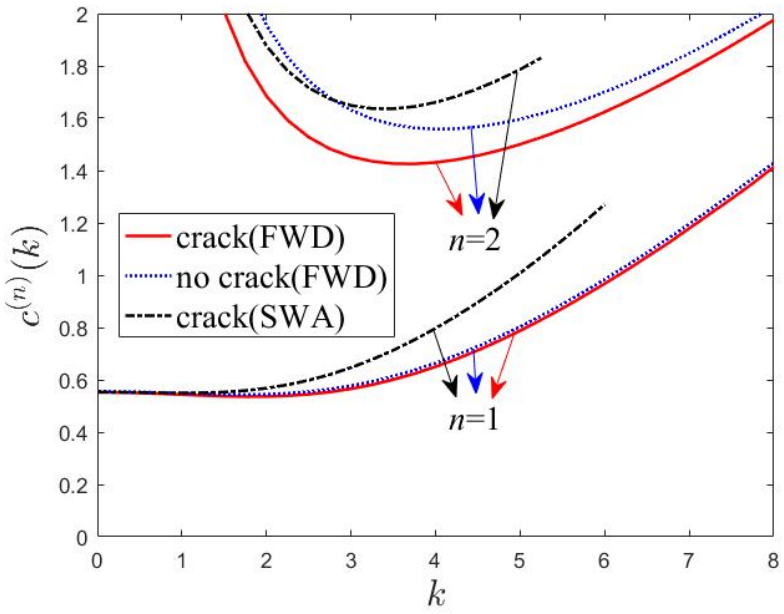

(a)

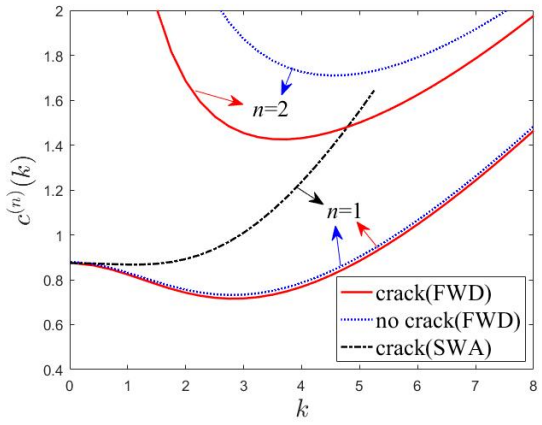

(b)

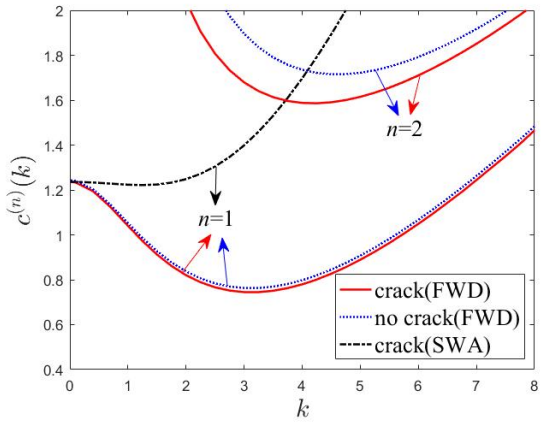

(c)

Figure 3: The phase speeds of even hydroelastic waves propagating in the ice channel with and without the crack in the center plane of the channel for $h = 0.01$: (a) $H = 0.2$, (b) $H = 0.5$, (c) $H = 1$. (FWD represents the finite water depth model, and SWA represents the shallow water approximation.)

Table 2: The critical speeds, $c^{(1)}_{cr,2}$ and $c^{(1)}_{cr,1}$, for the ice channels with a crack in the center plane of the channel with the dimensionless water depth $H = 0.5$.

	$c^{(1)}_{cr,2}$	$c^{(1)}_{cr,1}$
$h = 0$ (no ice)	0.707	-
$h = 0.005$	0.795	0.525
$h = 0.01$	0.874	0.716
$h = 0.02$	1.048	1.027

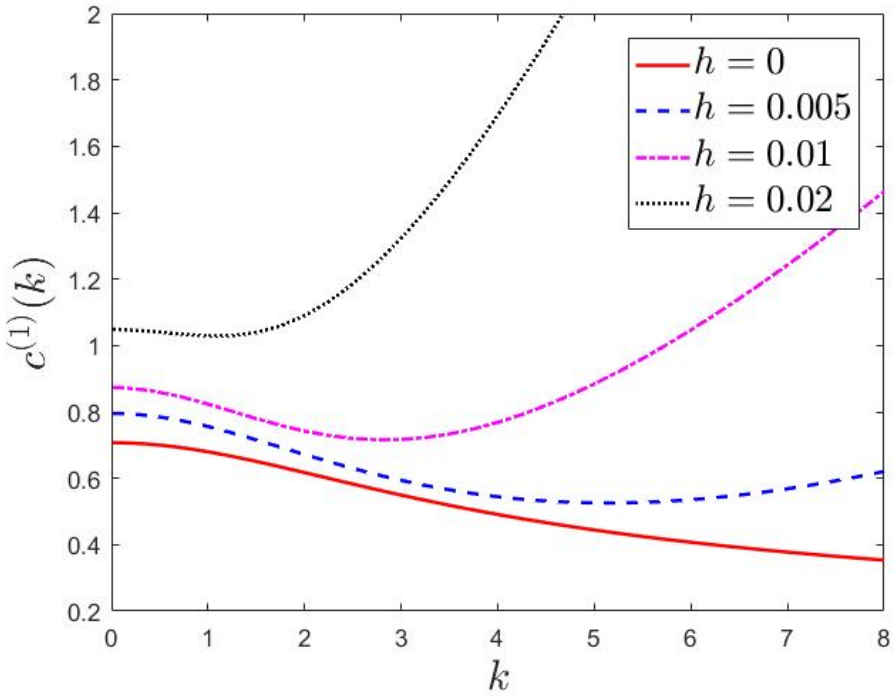

Figure 4: The phase speed of the lowest even hydroelastic wave propagating in the ice channel with a crack in the center plane of the channel for dimensionless water depth $H = 0.5$ and different ice thicknesses.

Table 3: The critical speeds, $c^{(1)}_{cr,1}$ and $c^{(2)}_{cr,1}$, for the ice channels with and without the crack in the center plane of the channel with the dimensionless ice thickness $h = 0.01$.

	$c^{(1)}_{cr,1}$ (crack)	$c^{(1)}_{cr,1}$ (no crack)	$c^{(2)}_{cr,1}$ (crack)	$c^{(2)}_{cr,1}$ (no crack)
$H = 0.2$	0.536	0.543	1.426	1.558
$H = 0.5$	0.716	0.732	1.579	1.709
$H = 1$	0.745	0.763	1.586	1.714

hydroelastic waves propagating at a speed close to $c^{(1)}_{cr,1}$. For ice sheet without a crack, figure 5(b) shows that $w^{(y=0)}_{\min}(\mathrm{Fr})$ and $w^{(y=0)}_{\max}(\mathrm{Fr})$ peak at Fr = 0.878 and Fr = 0.879, respectively, which are close to the critical speed of long waves for ice sheet without a crack, $c^{(1)}_{cr,2}$, for $H = 0.5$, see table 1. However, Shishmarev et al. [21] found that the maximum ice deflection occurs at the critical speed $c^{(1)}_{cr,1}$ for a load moving along the ice channel covered by viscoelastic ice sheet without crack. The reason is that a small water depth was considered in their study, where the critical speed of long waves, $c^{(1)}_{cr,2}$, and the critical speed of the first hydroelastic wave, $c^{(1)}_{cr,1}$, are close to each other. The comparison for maximum and minimum ice deflection between ice sheet with and without a crack are presented in figure 5(c) and 5(d). It is seen that the ice deflections for the ice sheet with a crack are greater than for the same ice sheet but without a crack.

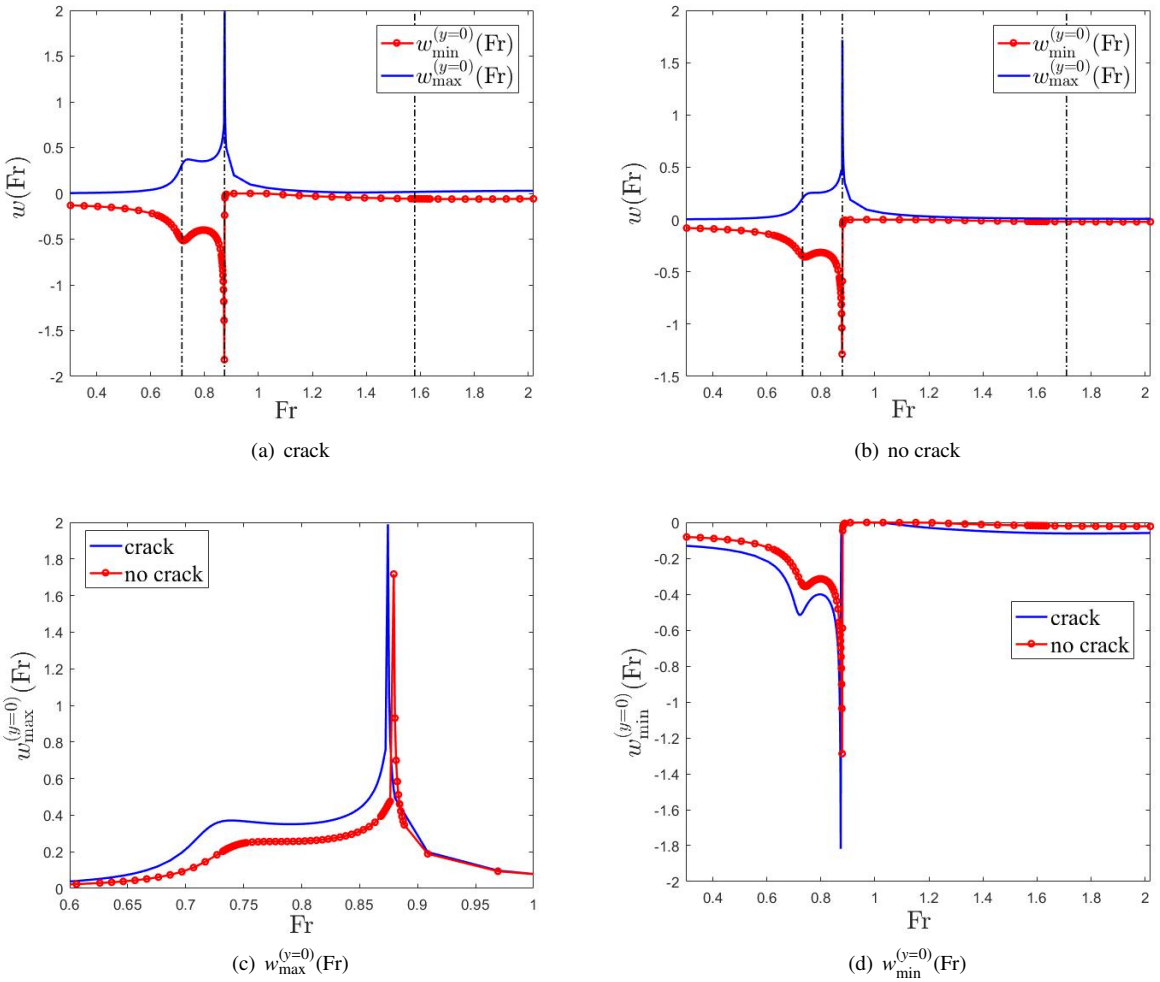

(a) crack (b) no crack

(c) $w^{(y=0)}_{\max}(\mathrm{Fr})$ (d) $w^{(y=0)}_{\min}(\mathrm{Fr})$

Figure 5: (a-b) The maximum and minimum of the dimensionless ice deflection, $w^{(y=0)}_{\max}(\mathrm{Fr})$ and $w^{(y=0)}_{\min}(\mathrm{Fr})$, along $y = 0$, as functions of the dimensionless load speed Fr. The dashed-dotted vertical lines are for the critical speeds, $c^{(1)}_{cr,1}$, $c^{(1)}_{cr,2}$ and $c^{(2)}_{cr,1}$. (c-d) The comparison of $w^{(y=0)}_{\max}(\mathrm{Fr})$ and $w^{(y=0)}_{\min}(\mathrm{Fr})$ for the ice sheet with and without a crack. Here $H = 0.5$, $h = 0.01$ and $\tau = 0.1$ s.

The maximum of the scaled strain in the ice sheet, $\epsilon_{\max}(\mathrm{Fr}) = \max_{|x|<\infty,|y|\le 1}\{\epsilon(x,y)\}$, the maximum of the scaled strain along $y = 0$, $\epsilon^{(y=0)}_{\max}(\mathrm{Fr}) = \max_{|x|<\infty}\{\epsilon(x,0)\}$, and the maximum of the scaled strain along the walls, $\epsilon^{(y=\pm1)}_{\max}(\mathrm{Fr}) = \max_{|x|<\infty}\{\epsilon(x,\pm1)\}$, as functions of the dimensionless load speed, Fr, are shown in figure 6 with and without a crack. For

ice sheet with a crack, figure 6(a) shows that $\epsilon_{\max}^{(y=0)}(\mathrm{Fr})$ peaks at $\mathrm{Fr}^* = 0.708$, which is close to but not equal to the critical speed $c_{cr,1}^{(1)}$. However, $\epsilon_{\max}(\mathrm{Fr})$ and $\epsilon_{\max}^{(y=\pm1)}(\mathrm{Fr})$ peak exactly at the critical speed $c_{cr,2}^{(1)}$. The maximum strain of the ice plate $\epsilon_{\max}(\mathrm{Fr})$ is equal to $\epsilon_{\max}^{(y=0)}(\mathrm{Fr})$ for dimensionless load speed smaller than $\mathrm{Fr}^* = 0.708$, and is equal to $\epsilon_{\max}^{(y=\pm1)}(\mathrm{Fr})$ for load speed greater than $\mathrm{Fr}^* = 0.708$. Thus, it can be concluded that the ice sheet is more likely to be further fractured along the crack for load speed smaller than Fr^*, and the connection between the ice sheet and channel walls is more easier to be broken for load speed greater than Fr^*, where Fr^* is close to but not equal to the dimensionless critical speed $c_{cr,1}^{(1)}$ for $\tau = 0.1$ s. For ice sheet without a crack, similar conclusions also can be obtain, see figure 6(b). But the strain along $y = 0$, $\epsilon_{\max}^{(y=0)}(\mathrm{Fr})$, peaks at the critical speed $c_{cr,2}^{(1)}$, see figure 6(b) and 6(c). The strain along $y = 0$ for ice sheet with and without crack are approximately equal to each other for dimensionless load speed $\mathrm{Fr} \geq 1.4$ and $\tau = 0.1$ s. The stain along the channel walls for ice sheet with and without crack are approximately equal to each other for dimensionless load speed $0.3 \leq \mathrm{Fr} \leq 2.02$ and $\tau = 0.1$ s, see figure 6(d).

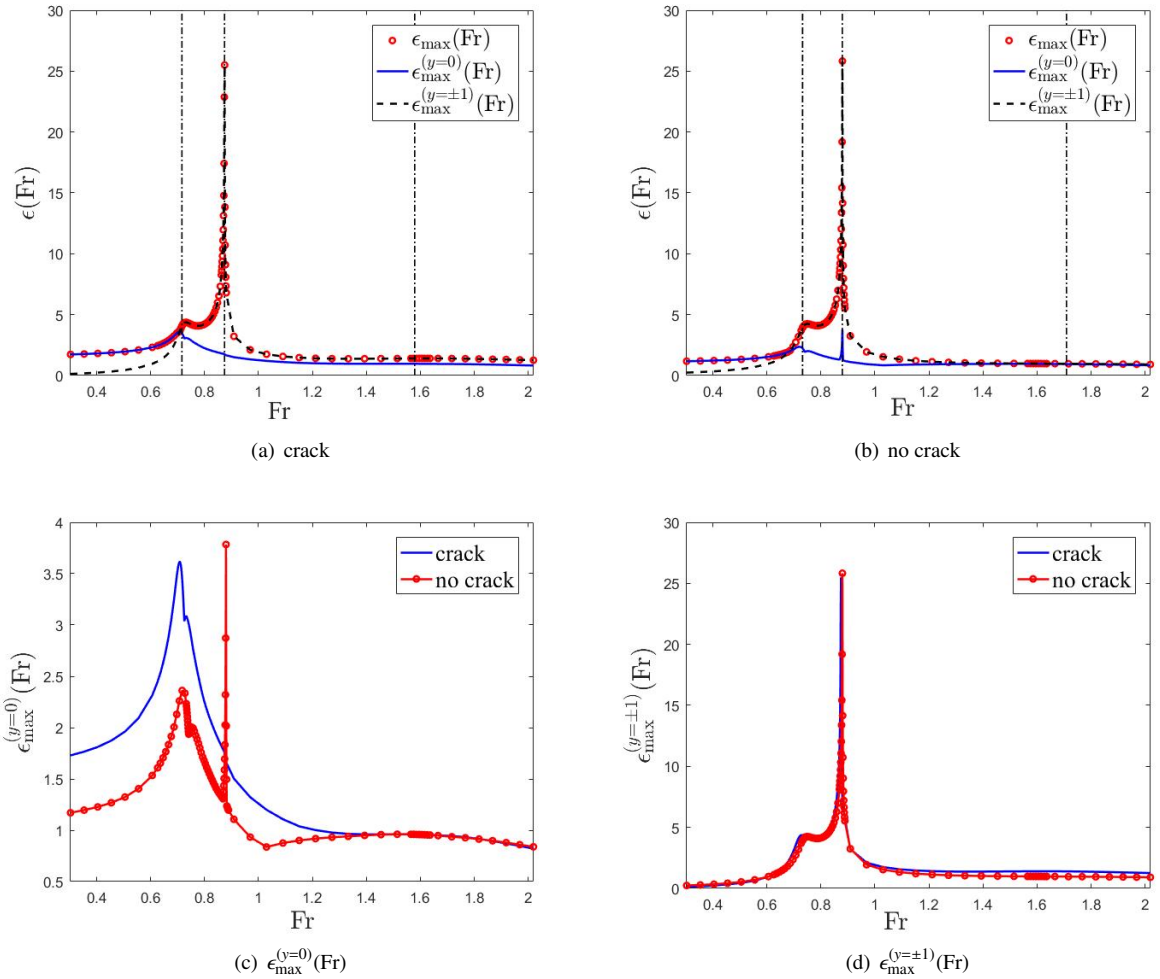

(a) crack (b) no crack

(c) $\epsilon_{\max}^{(y=0)}(\mathrm{Fr})$ (d) $\epsilon_{\max}^{(y=\pm1)}(\mathrm{Fr})$

Figure 6: (a-b) The maximum of the scaled strain in the ice sheet, $\epsilon_{\max}(\mathrm{Fr})$, the maximum of the scaled strain along $y = 0$, $\epsilon_{\max}^{(y=0)}(\mathrm{Fr})$, and the maximum of the scaled strain along walls of the channel, $\epsilon_{\max}^{(y=\pm1)}(\mathrm{Fr})$, as functions of the dimensionless load speed. The dashed-dotted vertical lines are for the critical speeds, $c_{cr,1}^{(1)}$, $c_{cr,2}^{(1)}$ and $c_{cr,1}^{(2)}$. (c-d) The comparison of $\epsilon_{\max}^{(y=0)}(\mathrm{Fr})$ and $\epsilon_{\max}^{(y=\pm1)}(\mathrm{Fr})$ for the ice sheet with and without a crack. Here $H = 0.5$, $h = 0.01$ and $\tau = 0.1$ s.

In the above analysis, we have known that the maximum and minimum of the dimensionless ice deflection occur at $\mathrm{Fr} = 0.874$ and $\mathrm{Fr} = 0.873$, respectively. It is interesting to investigate the plate deflections for the load moving with

these two speeds. Figures 7(a) and 7(c) show that the three-dimensional ice deflections differ significantly for these two dimensionless speeds, even though their values differ only by 0.001. For the dimensionless load speed Fr = 0.873, see figure 7(b), the ice deflection along the crack oscillates in front of the load with a very short wavelength, while the oscillations behind the load have longer wavelength. For the dimensionless load speed Fr = 0.874, which is equal to the critical speed $c^{(1)}_{cr,2}$ at $k \to 0$, there are no oscillations for the ice sheet behind the moving load but the ice deflections keep negative for $x < -20$, see figure 7(d). Note that the dimensionless ice deflection under the load is $w(0,0) = 2$, see figure 7(d), which means that the ice sheet is elevated under the load, which may have an obvious effect on operations of structures moving in an ice channel with a crack.

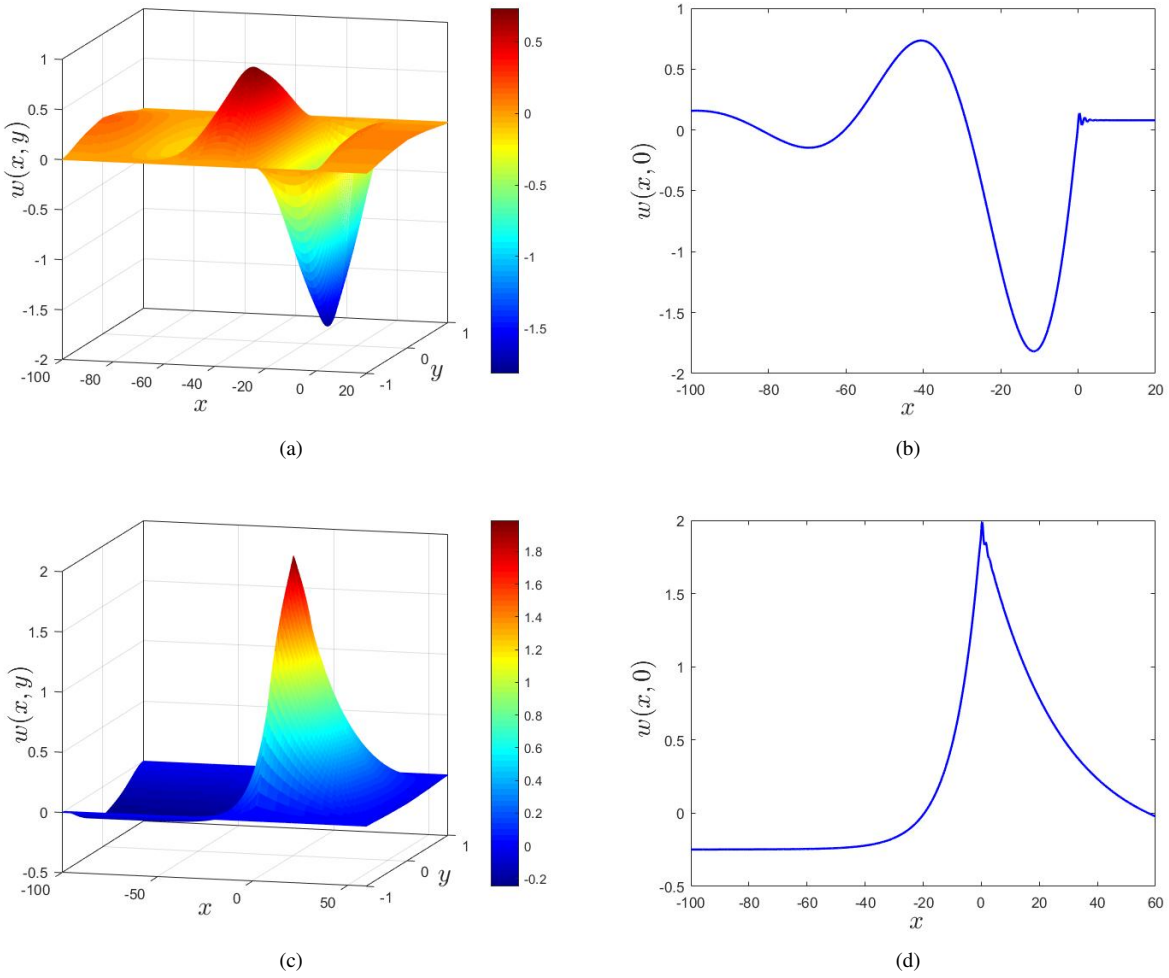

Figure 7: Three-dimensional ice deflections and ice deflections along the crack for dimensionless load speeds, (a-b) Fr = 0.873 and (c-d) Fr = 0.874. Here $H = 0.5$, $h = 0.01$ and $\tau = 0.1$ s.

The dimensionless ice deflection and scaled strain along the crack, $y = 0$, and along the walls, $y = \pm 1$, are shown as functions of the dimensionless longitudinal coordinate x along the channel for a subcritical speed in figure 8 and for a supercritical speed in figure 9, where the dimensional retardation times of the ice are $\tau = 1$ s, 0.1 s and 0.01 s. The characteristics of the ice responses shown in figures 8 and 9 can be explained in terms of the phase speeds of the hydroelastic waves, see figure 3. The ice responses are localised near the load moving at a subcritical speed, the hydroelastic waves do not exist for load speeds smaller than the critical speed $c^{(1)}_{cr,1}$. The hydroelastic waves contribute to the ice response for supercritical speed, see figure 9. For supercritical speed Fr = 0.909, only the first even hydroelastic wave ($n = 1$) with the dimensionless wave number $k \approx 5.2$ has phase speed equal to the load speed,

see figure 2. This wave number corresponds to the dimensionless wave length of 1.21, which is equal to the distance between two subsequent peaks of ice deflection in figure 9. Note that the amplitude of dimensionless strains decay with the distance from the load due to the damping in the ice sheet, see figure 9(b) and 9(c). The damping is described by the retardation time of ice, τ. The effect of the retardation time τ on the deflections and strains in the ice sheet is also demonstrated in figure 8 and 9. The decrease of the retardation time of ice increases the maximum strains. From figure 8, we can find that the minimum deflection of the ice sheet at $y = 0$ is not exactly under the load, but at a some distance behind the load. This lag of the position of the minimum ice deflection was measured by Takizawa [11] and was used to estimate the viscoelastic characteristics of the ice. The extent of the significant ice deflection decreases with increase of the retardation time of ice for supercritical speeds, see figure 9.

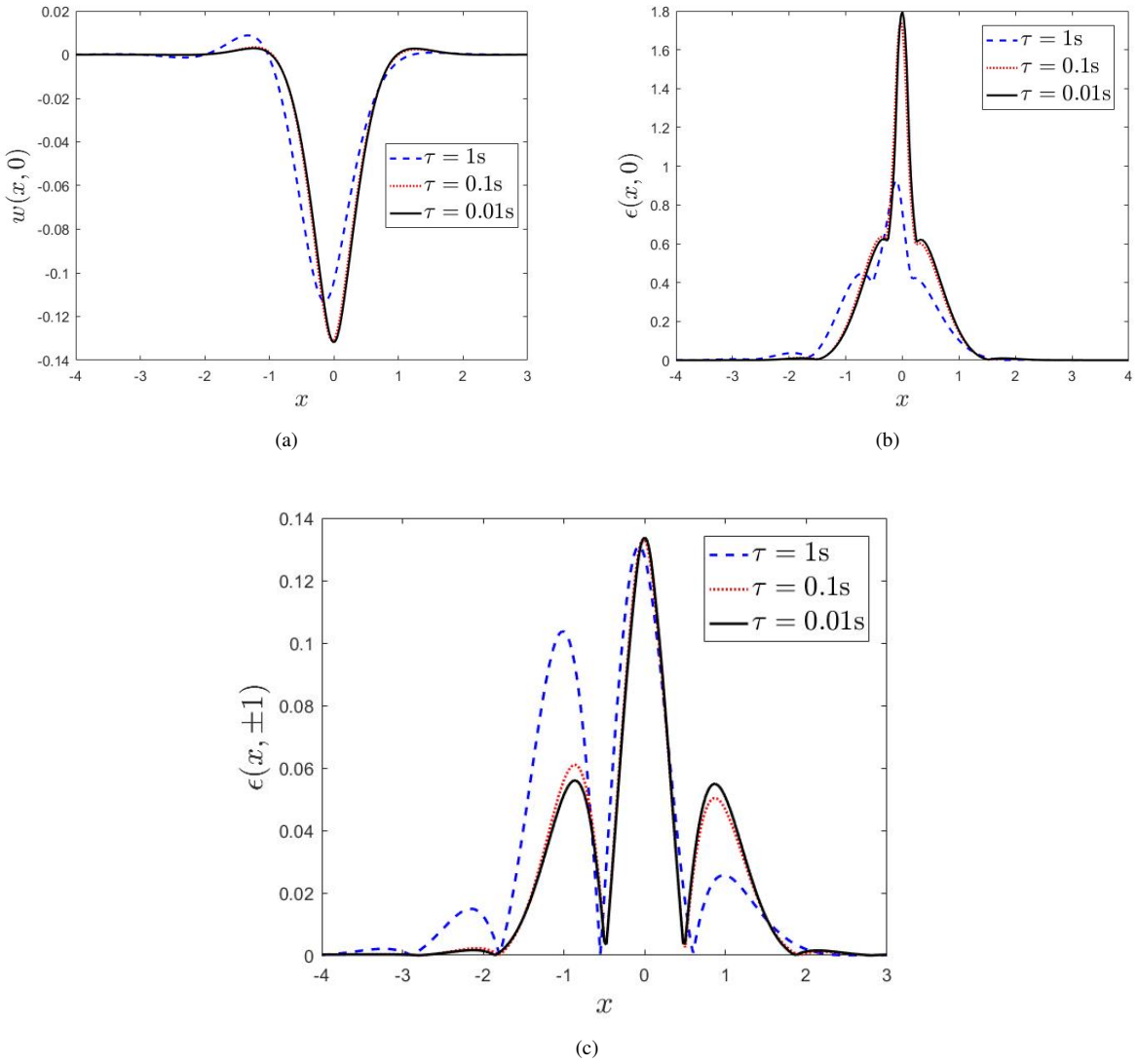

Figure 8: The dimensionless ice deflections (a) and scaled strains (b, c) caused by the load moving with the subcritical speed Fr = 0.303 for different values of the ice retardation time. Here $H = 0.5$ and $h = 0.01$.

The maximum and minimum of the dimensionless ice deflection, $w_{\max}^{(y=0)}(\mathrm{Fr})$ and $w_{\min}^{(y=0)}(\mathrm{Fr})$, as functions of the dimensionless load speed, are shown in figure 10 for dimensional retardation time $\tau = 0.01$ s and $\tau = 0.001$ s. Figure 10 and figure 5(a), where $\tau = 0.1$ s, demonstrate that the ice responses near the critical speed $c_{cr,1}^{(1)}$ strongly depend

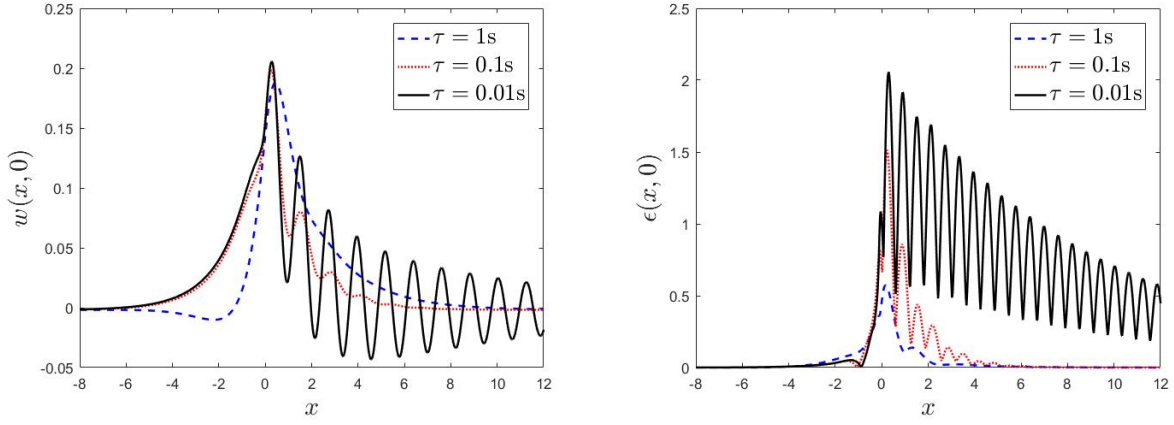

(a)

(b)

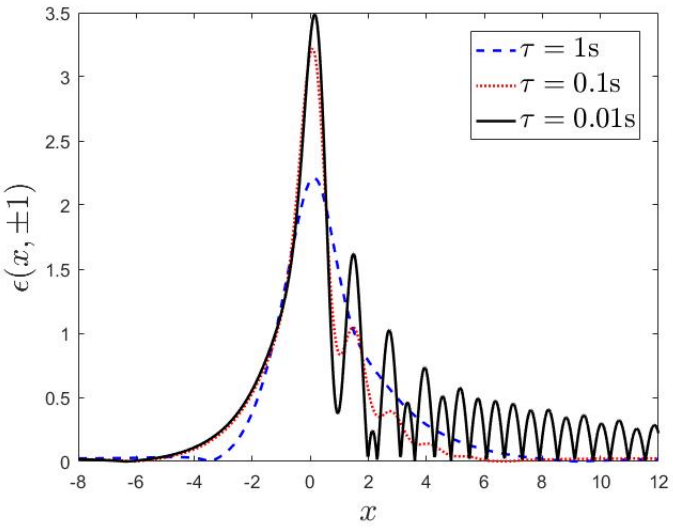

(c)

Figure 9: The dimensionless ice deflections (a) and scaled strains (b, c) caused by the load moving with the supercritical speed Fr = 0.909 for different values of the ice retardation time. Here $H = 0.5$ and $h = 0.01$.

on the retardation time of ice. The deformation amplitude of ice sheet increases with retardation time decrease at the critical speed $c^{(1)}_{cr,1}$. Note that the amplitude of the ice deflection at $c^{(1)}_{cr,1}$ exceeds that at $c^{(1)}_{cr,2}$ for the dimensional retardation time $\tau = 0.001$ s. The critical speed of the second hydroelastic wave, $c^{(2)}_{cr,1}$, is detected for dimensional retardation time $\tau = 0.001$ s, see figure 10(b). However, the amplitude of the ice deflection at $c^{(2)}_{cr,1}$ is relatively small compared with that at $c^{(1)}_{cr,1}$ and $c^{(1)}_{cr,2}$. Note that $w^{(y=0)}_{\max}(\mathrm{Fr})$ and $w^{(y=0)}_{\min}(\mathrm{Fr})$ oscillate for the load speed between $c^{(1)}_{cr,1}$ and $c^{(1)}_{cr,2}$ and $\tau = 0.001$ s, see figure 10(b). The maxima of the scaled strain as functions of the dimensionless load speed are shown in figure 11 for retardation time $\tau = 0.01$ s and $\tau = 0.001$ s. Figure 11 and figure 6(a), where $\tau = 0.1$ s, demonstrate that the strains near the critical speed $c^{(1)}_{cr,1}$ strongly depend on the retardation time of ice. The maxima of the strain increases with retardation time decrease at the critical speed $c^{(1)}_{cr,1}$, $c^{(1)}_{cr,2}$ and $c^{(2)}_{cr,1}$. The speed Fr^* at which the ice sheet is most likely to be broken along the crack or along the walls of the channel, is exactly equal to $c^{(1)}_{cr,1}$ for retardation time $\tau = 0.01$ s and $\tau = 0.001$ s and smaller than $c^{(1)}_{cr,1}$ for retardation time $\tau = 0.1$ s, which also proves that the retardation time of ice affects the critical speed $c^{(1)}_{cr,1}$ (Xue et al. [17]).

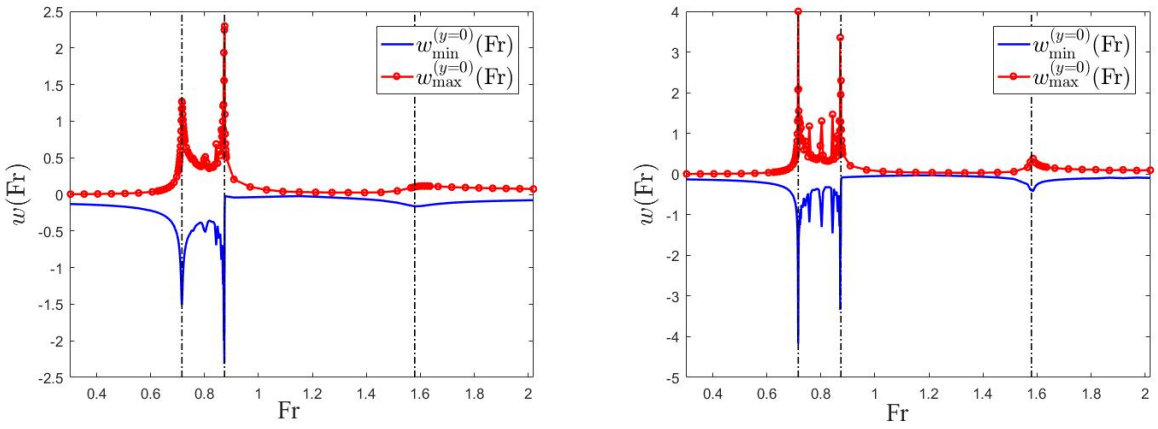

Figure 10: The maximum and minimum of the dimensionless ice deflection, $w^{(y=0)}_{\max}(\mathrm{Fr})$ and $w^{(y=0)}_{\min}(\mathrm{Fr})$, along the crack of the ice sheet as functions of the dimensionless load speed. Here $H = 0.5$, $h = 0.01$, (a) $\tau = 0.01$ s and (b) $\tau = 0.001$ s . The dashed-dotted vertical lines are for the critical speeds of this channel, $c^{(1)}_{cr,1}$, $c^{(1)}_{cr,2}$ and $c^{(2)}_{cr,1}$.

The maximum and minimum of the dimensionless ice deflection, $w^{(y=0)}_{\max}(\mathrm{Fr})$ and $w^{(y=0)}_{\min}(\mathrm{Fr})$, as functions of the dimensionless load speed, are shown in figure 12 for dimensionless ice thickness $h = 0.005$ and $h = 0.02$. Here the dimensional retardation time is $\tau = 0.1$ s. Figure 12(a) and figure 5(a) demonstrate that $w^{(y=0)}_{\max}(\mathrm{Fr})$ peaks at the critical speeds $c^{(1)}_{cr,2}$, and peaks locally near the critical speed $c^{(1)}_{cr,1}$ for dimensionless ice thickness $h = 0.005$ and $h = 0.01$. The ice deflection for $h = 0.02$ increases monotonically with increase of the load speed Fr and peaks near the critical speed $c^{(1)}_{cr,2}$, then decreases monotonically with increase of the load speed. Note that the critical speeds $c^{(1)}_{cr,2}$ and $c^{(1)}_{cr,1}$ are close to each other for this ice thickness. The maxima of the non-scaled strain as functions of the dimensionless load speed are shown in figure 13 for dimensionless ice thickness $h = 0.005$, 0.01 and 0.02. It is seen that the strains along the crack peak near the critical speed $c^{(1)}_{cr,1}$, which decreases with the ice thickness increases. The strains along the walls of the channel peak near the critical speed of long waves $c^{(1)}_{cr,2}$, which decreases with the ice thickness increases. Note that the maximum stains along the crack are approximately constant for dimensionless ice thickness $h = 0.02$ and load moving in the region of subcritical speed. It increases rapidly when the load speed approaches the critical speed $c^{(1)}_{cr,1}$. This means that finding the critical speed of the ice plate is essential to improve the ice breaking ability of the moving load, especially for thicker ice.

The dimensionless deflection of the ice sheet and the non-scaled strain in the ice sheet as functions of the dimensionless longitudinal coordinate x are presented in figure 14 and 15 for dimensionless load speeds $\mathrm{Fr} = 0.303$ and

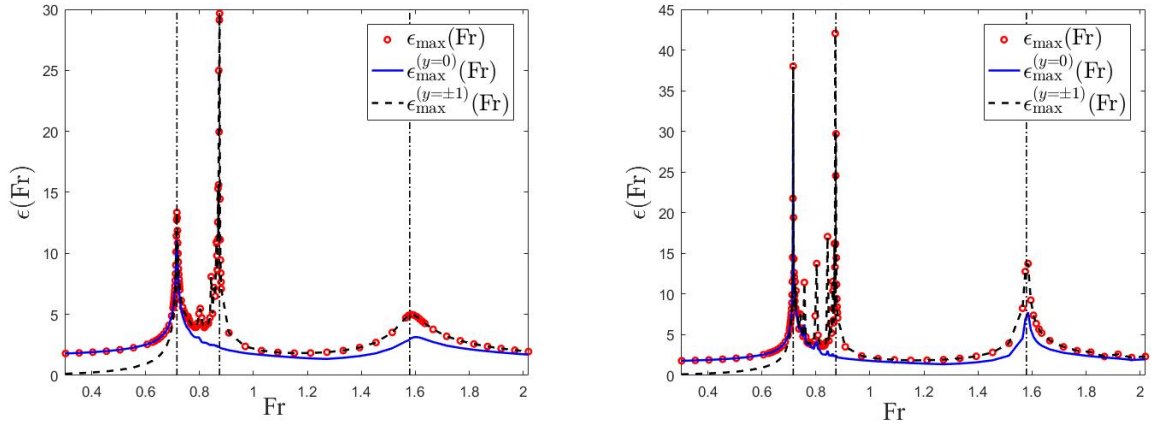

(a) (b)

Figure 11: The maximum of the scaled strain in the ice sheet, $\epsilon_{\max}(\mathrm{Fr})$, the maximum of the scaled strain along the crack of the ice sheet, $\epsilon_{\max}^{(y=0)}(\mathrm{Fr})$, and the maximum of the scaled strain along walls of the channel, $\epsilon_{\max}^{(y=\pm1)}(\mathrm{Fr})$, as functions of the load speed. Here $H = 0.5$, $h = 0.01$, (a) $\tau = 0.01$ s and (b) $\tau = 0.001$ s. The dashed-dotted vertical lines are for the critical speeds of this channel, $c_{cr,1}^{(1)}$, $c_{cr,2}^{(1)}$ and $c_{cr,1}^{(2)}$.

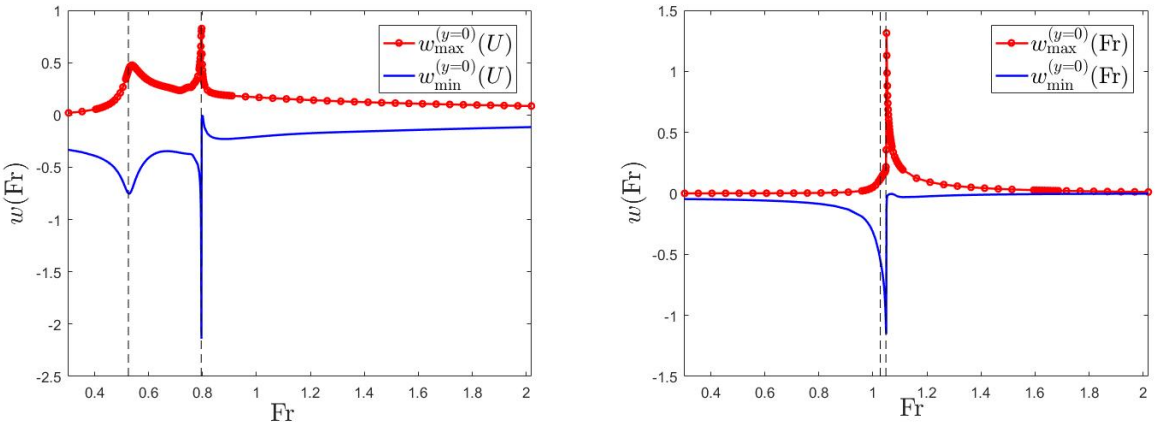

(a) (b)

Figure 12: The maximum and minimum of the dimensionless ice deflection, $w_{\max}^{(y=0)}(\mathrm{Fr})$ and $w_{\min}^{(y=0)}(\mathrm{Fr})$, along the crack of the ice sheet as functions of the dimensionless load speed. Here $H = 0.5$, $\tau = 0.1$ s, (a) $h = 0.005$ and (b) $h = 0.02$. The dashed vertical lines are for the critical speeds of this channel, $c_{cr,1}^{(1)}$ and $c_{cr,2}^{(1)}$.

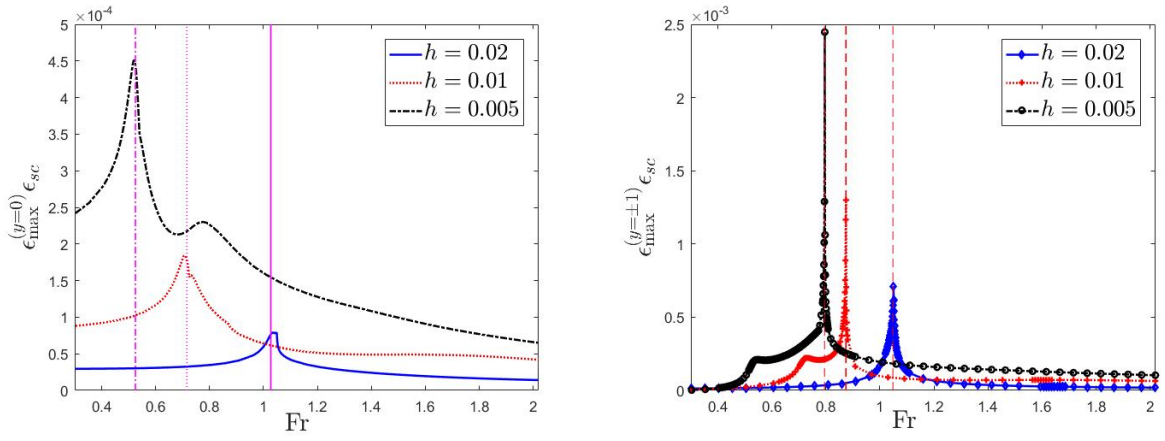

(a) (b)

Figure 13: The maximum of the non-scaled strain along the crack (a) and along the walls of the channel (b), as functions of the load speed for $H = 0.5$, $\tau = 0.1$ s and different ice thickness h. The vertical lines represent the corresponding critical speeds $c^{(1)}_{cr,1}$ (a) and $c^{(1)}_{cr,2}$ (b) for different ice thickness.

Fr = 0.909 and different ice thicknesses. Note that Fr = 0.303 is the subcritical speed for dimensionless ice thickness $h = 0.005$, $h = 0.01$ and $h = 0.02$. The localised ice response near the load decrease with the ice thickness increase, see figure 14(a) and 14(b). However, the strains at the channel walls increase with the ice thickness increase, which indicates the effect of channel walls is more important when the ice thickness is large. The dimensionless load speed Fr = 0.909 is supercritical for dimensionless ice thickness $h = 0.005$ and $h = 0.01$, and subcritical for $h = 0.02$. This is also clear from figure 15, where the ice response is localised for dimensionless ice thickness $h = 0.02$ and hydroelastic waves contribute to the ice response for $h = 0.005$ and $h = 0.01$.

The maximum and minimum of the dimensionless ice deflection, $w^{(y=0)}_{\max}(\mathrm{Fr})$ and $w^{(y=0)}_{\min}(\mathrm{Fr})$, as functions of the dimensionless load speed, are shown in figure 16 for dimensionless water depth $H = 0.2$ and $H = 1$. The dimensionless ice thickness $h = 0.01$. The dimensional retardation time $\tau = 0.1$ s. Figure 16 and figure 5(a) demonstrate that $w^{(y=0)}_{\max}(\mathrm{Fr})$ peaks at the critical speed $c^{(1)}_{cr,2}$ for different water depth of the channel. The maxima of the non-scaled strain as functions of the dimensionless load speed are shown in figure 17 for dimensionless water depth $H = 0.2$, 0.5 and 1. The strains along the crack peak near the critical speed $c^{(1)}_{cr,1}$, which decreases with the water depth increases. The strains along the walls of the channel peak near the critical speed of long wave $c^{(1)}_{cr,2}$, which decreases with the water depth increases. Thus, it can be concluded that the moving load has a stronger ice breaking ability in a small water depth channel. In other words, moving loads are more suitable for ice breaking in ice regions with a small water depth.

The ice response is proportional to the magnitude of the load within the linear model of hydroelasticity. By using the obtained deflections and strains, it is not complicated to find the ice response to any given load magnitude. However, one may expect that the aspect-ratio of the load, a/b, where a is the dimensionless length of the load along the channel and b is the dimensionless width of the load, has a certain effect on ice deflections and strains. To investigate this effect, we let the dimensionless width of the load b and pressure amplitude P_0 change but keep the total load $4P_0ab$ constant. The maxima of the non-scaled strain along the crack and along the walls of the channel as functions of the dimensionless load speed are presented in figure 18 for $a/b = 2$, 1 and 0.5. The strains along the crack peak near the critical speed $c^{(1)}_{cr,1}$, which increases with the aspect-ratio of the load a/b increases. The strains along the walls of the channel peak near the critical speed of long wave $c^{(1)}_{cr,2}$, which increases with the aspect-ratio of the load a/b increases.

Figure 19 and 20 show the strain maxima as functions of the length of the load a and the width of the load b for different load speeds respectively. The total load $4P_0ab$ is constant. For a given total load and width of the load b, the maximum strain decreases with length of the load a increases. This means that the ice sheet is harder to be broken if

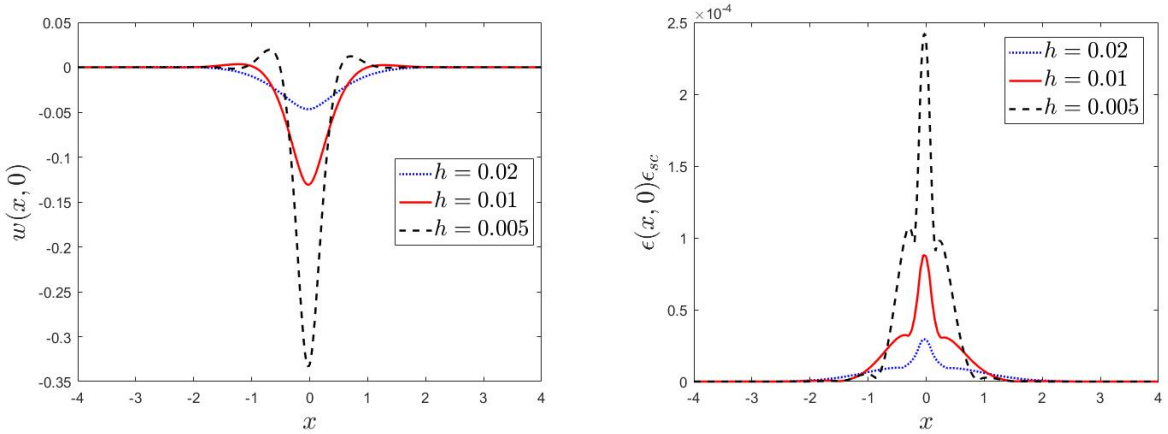

(a)

(b)

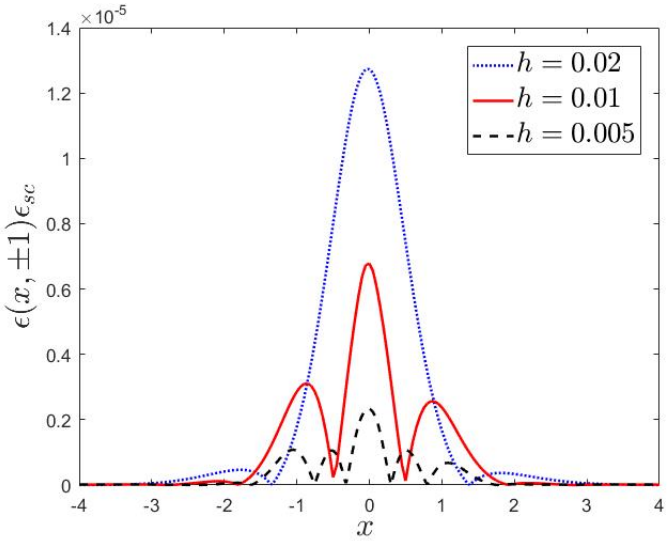

(c)

Figure 14: The dimensionless ice deflections (a) and strains (b, c) caused by the load moving with the subcritical speed Fr = 0.303 for different values of the dimensionless ice thickness. Here $H = 0.5$ and $\tau = 0.1$ s.

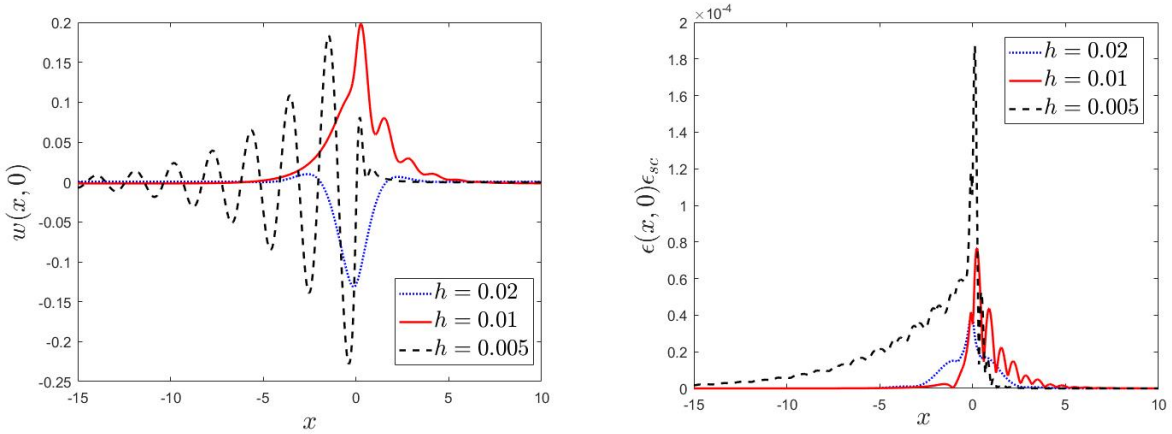

(a) (b)

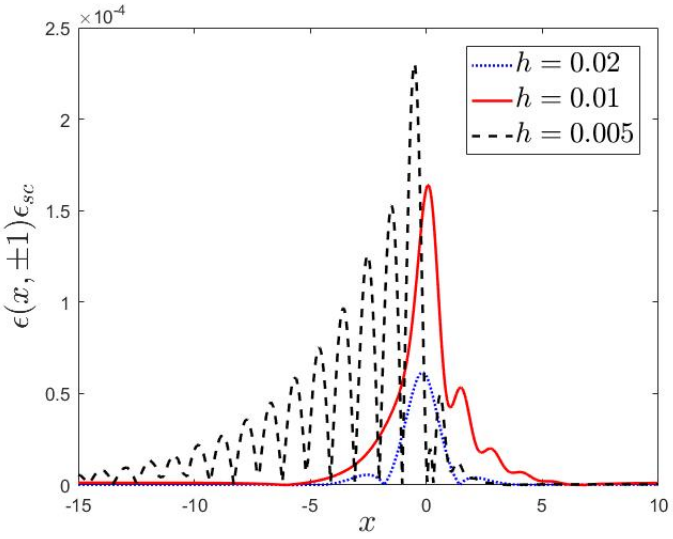

(c)

Figure 15: The dimensionless ice deflections (a) and strains (b, c) caused by the load moving with the speed Fr = 0.909 for different values of the dimensionless ice thickness. Here $H = 0.5$ and $\tau = 0.1$ s.

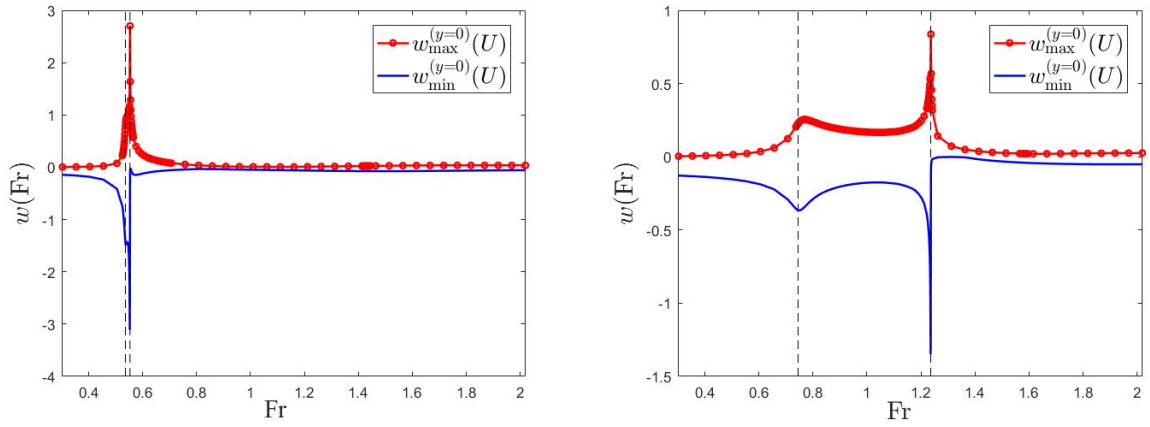

(a) (b)

Figure 16: The maximum and minimum of the dimensionless ice deflection, $w_{\max}^{(y=0)}(\mathrm{Fr})$ and $w_{\min}^{(y=0)}(\mathrm{Fr})$, along the crack of the ice sheet as functions of the dimensionless load speed. Here $h = 0.01$, $\tau = 0.1$ s, (a) $H = 0.2$ and (b) $H = 1$. The dashed vertical lines are for the critical speeds of this channel, $c_{cr,1}^{(1)}$ and $c_{cr,2}^{(1)}$.

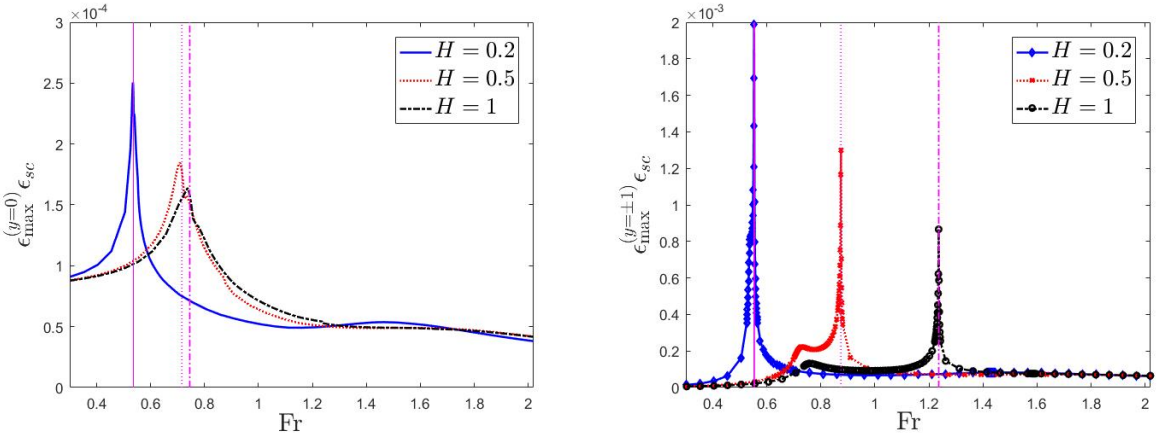

(a) (b)

Figure 17: The maximum of the non-scaled strain along the crack (a) and along the walls of the channel (b), as functions of the load speed for $h = 0.01$, $\tau = 0.1$ s and different water depth H. The vertical lines represent the corresponding critical speeds $c_{cr,1}^{(1)}$ (a) and $c_{cr,2}^{(1)}$ (b) for different water depth.

the load is elongated along the ice channel for a given width of the load. The ice breaking ability of a load moving with a constant speed will drop rapidly when the load length a exceeds the given load width b, see figure 19(a). For a given total load and length of the load a, the maximum strain increases with width of the load b decreases. This means that the ice sheet is easier to be broken if the load is elongated along the ice channel for a given length of the load. It also should be mentioned that the ice breaking ability of a load moving with a constant speed does not continue to distinctly increase if the width of the moving load, b, is ten times less than the given load length a, see figure 20.

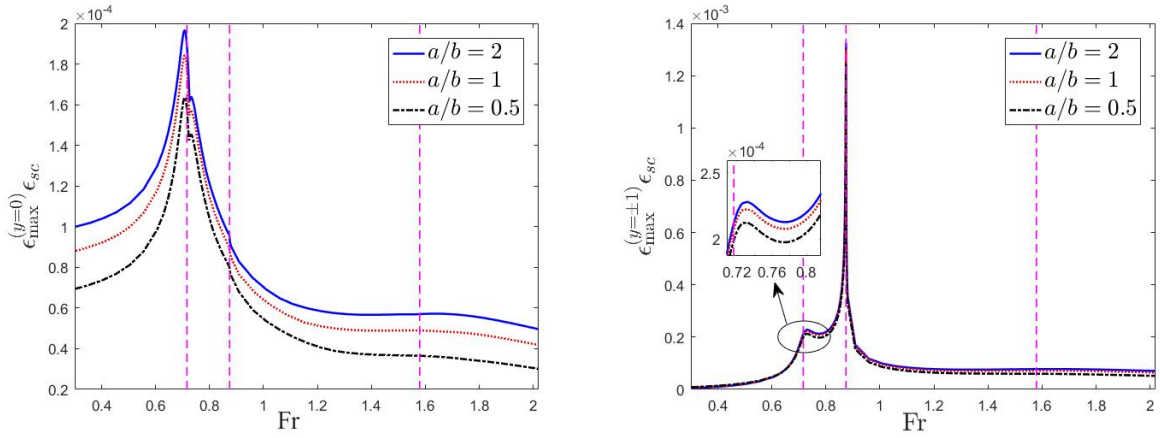

(a) (b)

Figure 18: The maximum of the non-scaled strain along the crack (a) and the maximum of the non-scaled strain along walls of the channel (b), as functions of the load speed for $H = 0.5$, $h = 0.01$, $\tau = 0.1$ s and different aspect-ratio of the load a/b. The total load $4P_0ab = 4000$ N is constant. The dashed vertical lines are for the critical speeds of this channel, $c^{(1)}_{cr,1}$, $c^{(1)}_{cr,2}$ and $c^{(2)}_{cr,1}$.

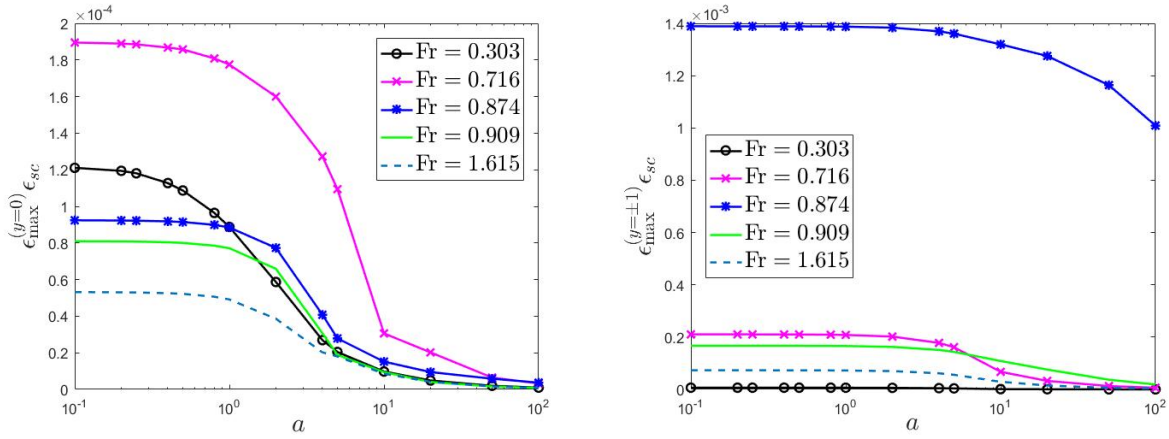

(a) (b)

Figure 19: The maxima of the non-scaled strains along the crack (a) and along the walls of the channel (b) as functions of a for different load speeds. Here $P_0 = 1000$ Pa, $b = 1$ m, $H = 0.5$, $h = 0.01$ and $\tau = 0.1$ s. The total load $4P_0ab = 4000$ N is constant.

5. Conclusions

The response of an ice-covered channel with a crack in the center plane of the channel to a load moving on the ice sheet has been studied. The formulated problem was solved by using the Fourier transform along the channel and the

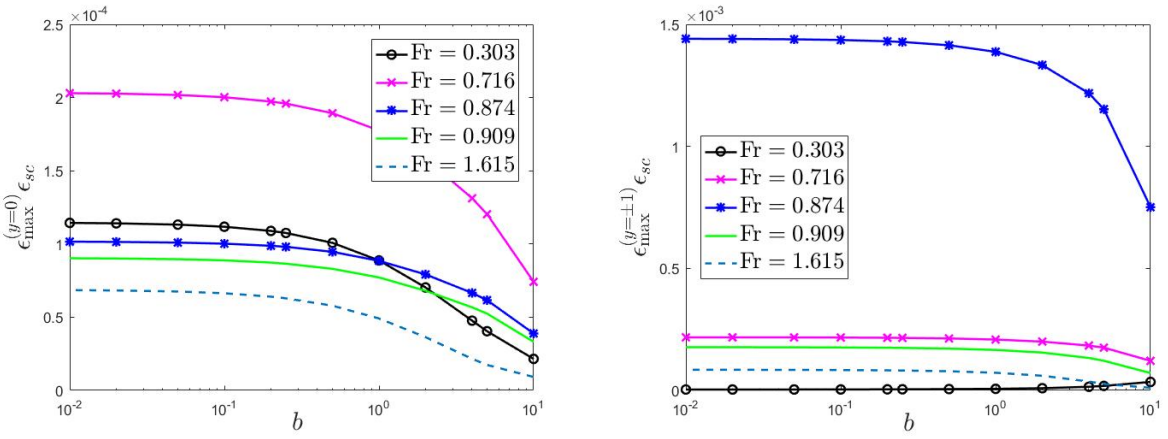

Figure 20: The maxima of the non-scaled strains along the crack (a) and along the walls of the channel (b) as functions of b for different load speeds. Here $P_0 = 1000$ Pa, $a = 1$ m, $H = 0.5$, $h = 0.01$ and $\tau = 0.1$ s. The total load $4P_0ab = 4000$ N is constant.

normal mode method across the channel. The ice sheet was modeled by viscoelastic Kelvin-Voigt plate. Only uniform and rectangular loads symmetric with respect to the center plane of the channel were considered. It was shown that the response of the ice sheet to a moving load strongly depends on the relation between the load speed and the critical speeds of the hydroelastic waves propagating along the channel. The characteristics of ice response were classified in terms of the critical speeds of the hydroelastic waves. The ice response is localised near the moving load for load speed U smaller than $c^{(1)}_{cr,1}$. For load speed between $c^{(1)}_{cr,1}$ and $c^{(1)}_{cr,2}$, the ice deflection oscillates both in front of and behind the load. These oscillations correspond to the first even hydroelastic wave with the phase speed equal to the speed of the load. As the speed of the load continues to increase and becomes between $c^{(1)}_{cr,2}$ and $c^{(2)}_{cr,1}$, the ice sheet only oscillates in front of the load.

The ice responses strongly depend on the retardation time. It was shown that, for relatively small retardation time, both the ice deflection and strain along the crack peak at the critical speed $c^{(1)}_{cr,1}$. For relatively large retardation time, the strains along the crack achieve their maximum for load speed close to but not equal to the critical speed $c^{(1)}_{cr,1}$. However, the ice deflection along the crack peaks exactly at the critical speed $c^{(1)}_{cr,2}$. The strain along the center of the channel peaks at the critical speed of long waves, $c^{(1)}_{cr,2}$, for ice sheet without a crack, while it peaks near the critical speed, $c^{(1)}_{cr,1}$, for ice sheet with a crack. As the ice thickness increases, the maximum strain along the crack decreases dramatically. In order to improve the ice breaking ability of the moving load, it is essential to find the critical speed of the ice plate, especially for thicker ice. The maximum magnitude of both the ice deflection and strain along the crack decrease with increase of the depth of the channel. This implies that the ice sheet in a channel of smaller depth is more likely to be broken for the same load. For a given total load and width of the load, the more the load is elongated along the channel, the smaller the ice strain in the ice sheet. The ice sheet is harder to be broken if the load is elongated along the channel.On the other hand, for a given total load and length of the load, the more the load is elongated along the channel, the larger the ice strain in the ice sheet. The ice sheet is easier to be broken if the load is elongated along the channel.

The maximum of the strain in the ice sheet is achieved along the crack for the load speed U smaller than the critical speed $c^{(1)}_{cr,1}$, but on the channel walls for load speed greater than the critical speed $c^{(1)}_{cr,1}$. This implies that if a load moves with a supercritical speed, $U \geq c^{(1)}_{cr,1}$, the connection between the ice sheet and the channel walls would be broken first. If the ice sheet is detached from the walls, the edge conditions (12) should be changed to (3) at the channel walls $y = \pm 1$, which change the boundary conditions at $y = 1$ in (18) to

$$\psi_n''(1) = \nu\xi^2\psi_n(1), \quad \psi_n'''(1) = (2-\nu)\xi^2\psi_n'(1). \tag{30}$$

If a load moves with a subcritical speed, $U < c_{cr,1}^{(1)}$, the ice sheet would be damaged along the crack.

Acknowledgements

This work was supported by the National Natural Science Foundation of China (Nos. 51979051, 51979056 and 51639004), to which the authors are most grateful.

Appendix A. The integrals $C_{kn}(\xi)$

The method of separating variables applied to the boundary problem (23) and (24) provides

$$\Phi_n(y,z,\xi) = \sum_{m=1}^{\infty} D_{nm} \frac{\cosh[\sqrt{\xi^2+\mu_m^2}(z+H)]}{\cosh[\sqrt{\xi^2+\mu_m^2}H]} \cos(\mu_m y), \qquad \mu_m = \pi(m-1) \quad (m=1,2,3,..), \tag{A.1}$$

where the coefficients D_{nm} are determined using the boundary condition $\Phi_{n,z} = \psi_n(|y|)$ on $z = 0$,

$$\frac{\partial \Phi_n}{\partial z} = \sum_{m=1}^{\infty} D_{nm} \left(\sqrt{\xi^2+\mu_m^2} \tanh[\sqrt{\xi^2+\mu_m^2}H] \right) \cos(\mu_m y) = \psi_n(|y|). \tag{A.2}$$

The functions $\cos(\mu_m y)$, $m \geq 1$, are orthogonal in the interval $-1 < y < 1$,

$$\int_{-1}^{1} \cos(\mu_m y)\cos(\mu_r y)\mathrm{d}y = \begin{cases} 0, & r \neq m, \\ 1, & r = m \neq 1 \\ 2, & r = m = 1. \end{cases} \tag{A.3}$$

Multiplying both sides of (A.2) by $\cos(\mu_r y)$ and integrating the result in y from -1 to 1 using the relations (A.3), we find

$$D_{nm} = \frac{\epsilon_m}{\sqrt{\xi^2+\mu_m^2}\tanh[\sqrt{\xi^2+\mu_m^2}H]} \int_0^1 \psi_n(y)\cos(\mu_m y)\mathrm{d}y, \tag{A.4}$$

where $\epsilon_1 = 1$ and $\epsilon_m = 2$ for $m \geq 2$.

Denote the integrals in (A.4) by S_{nm}. Then equations (A.1) and (A.4) give the integrals

$$C_{nr}(\xi) = \int_0^1 \Phi_n(y,0,\xi)\psi_r(y)\mathrm{d}y = \sum_{m=1}^{\infty} \frac{\epsilon_m S_{nm} S_{rm}}{\sqrt{\xi^2+\mu_m^2}\tanh[\sqrt{\xi^2+\mu_m^2}H]}. \tag{A.5}$$

Note that $\mu_1 = 0$, then equation (A.5) is convenient to write as

$$C_{nr}(\xi) = \frac{S_{n1}S_{r1}}{\xi\tanh(\xi H)} + \sum_{m=2}^{\infty} \frac{2S_{nm}S_{rm}}{\sqrt{\xi^2+\mu_m^2}\tanh[\sqrt{\xi^2+\mu_m^2}H]}, \tag{A.6}$$

where the first term tends to ∞ as $\xi \to 0$ and the series is finite for $\xi \geq 0$. However, in equation (27) we need the product $\xi^2 C_{nr}(\xi)$, which has a finite limit as $\xi \to 0$,

$$\xi^2 C_{nr}(\xi) = \frac{S_{n1}S_{r1}}{H} \quad (\xi \to 0). \tag{A.7}$$

The integrals S_{nm} are evaluated by multiplying equation (19) by $\cos(\mu_m y)$ and integrating the result in y from 0 to 1. One find

$$S_{nm} = \begin{cases} \frac{(-1)^{m+1}\psi_n'''(1)+(\mu_m^2+\nu\xi^2)\psi_n'(0)}{\lambda_n^4-(\xi^2+\mu_m^2)^2} & (\xi^2 \neq \lambda_n^2-\mu_m^2), \\ \frac{(-1)^m\psi_n'''(1)Q(\lambda_n)-2\psi_n'(0)}{4\lambda_n^2} & (\xi^2 = \lambda_n^2-\mu_m^2), \end{cases} \tag{A.8}$$

where $Q(\lambda_n)$ is defined in section 3.

Appendix B. Asymptotic analysis of the spectral problem (18) as $\xi \to 0$

The asymptotic expansions of the solutions of the spectral problem (18) and the corresponding eigenvalues for small ξ are sought in the form, $\psi_n(y,\xi) = \psi_n^{(0)}(y) + O(\xi^2)$ and $\lambda_n(\xi) = \lambda_n^{(0)} + O(\xi^2)$, where $\psi_n^{(0)}(y)$ is the non-zero solutions of the problem

$$\frac{\mathrm{d}^4\psi_n^{(0)}}{\mathrm{d}y^4} = \left[\lambda_n^{(0)}\right]^4 \psi_n^{(0)} \quad (0 < y < 1). \tag{B.1}$$

with the boundary conditions

$$\psi_n^{(0)} = \left[\psi_n^{(0)}\right]' = 0 \quad (y = 1), \tag{B.2}$$

$$\left[\psi_n^{(0)}\right]'' = 0, \left[\psi_n^{(0)}\right]''' = 0 \quad (y = 0). \tag{B.3}$$

The orthogonality condition (20) gives

$$\int_0^1 \psi_n^{(0)}\psi_m^{(0)}\mathrm{d}y = \delta_{nm} \tag{B.4}$$

for any $n, m \geq 1$.

The solutions of the spectral problem (B.1)-(B.4) are known as the normal modes of a cantilever beam,

$$\psi_n^{(0)}(y) = A_n\left[(1 - e^{-\lambda_n^{(0)}}\theta^-)\sin(\lambda_n^{(0)}y) - (1 + e^{-\lambda_n^{(0)}}\theta^+)\cos(\lambda_n^{(0)}y) - \tanh(\lambda_n^{(0)})e^{-\lambda_n^{(0)}y} - \sin(\lambda_n^{(0)})e^{-\lambda_n^{(0)}(1-y)}\right], \tag{B.5}$$

where $A_n = 1/|\theta^- - e^{-\lambda_n^{(0)}}|$ and $\theta^{\pm} = \sin(\lambda_n^{(0)}) \pm \cos(\lambda_n^{(0)})$. The eigenvalues $\lambda_n^{(0)}$ are solutions of the dispersion equation,

$$\cos\lambda_n^{(0)} = -1/\cosh\lambda_n^{(0)}, \tag{B.6}$$

where $\lambda_n^{(0)} = \frac{\pi}{2}(2n-1) + \delta_n$, $n \geq 1$ and $\delta_n \to 0$ as $n \to \infty$. Equation (B.6) is solved by iterations, $\delta_n^{(i+1)} = (-1)^{(n+1)}\arcsin(1/\cosh(\frac{\pi}{2}(2n-1) + \delta_n^{(i)}))$, where i is the iretation number and $\delta_n^{(0)} = 0$.

The asymptotic expansions of S_{nm} in (A.8) as $\xi \to 0$ have the form

$$S_{nm} = S_{nm}^{(0)} + O(\xi^2), \tag{B.7}$$

where

$$S_{nm}^{(0)} = \frac{(-1)^{m+1}\left[\psi_n^{(0)}\right]'''(1) + \mu_m^2\left[\psi_n^{(0)}\right]'(0)}{\left[\lambda_n^{(0)}\right]^4 - \mu_m^4}. \tag{B.8}$$

Substituting (B.7) into (A.6), we obtain the asymptotic expansions of the products $\xi^2 C_{nr} = C_{nr}^{(0)} + O(\xi^2)$ with

$$C_{nr}^{(0)} = \frac{S_{n1}^{(0)}S_{r1}^{(0)}}{H}, \quad S_{r1}^{(0)} = \frac{-2\left(\theta^+ + e^{-\lambda_n^{(0)}}\right)}{\lambda_n^{(0)}|\theta^- - e^{-\lambda_n^{(0)}}|}. \tag{B.9}$$

The asymptotic expansions of the matrices $\xi^2\mathbf{C}$ and $\mathbf{B}$ in (27) are

$$\xi^2\mathbf{C} = \mathbf{C}^{(0)} + O(\xi^2), \tag{B.10}$$

$$\mathbf{B} = \mathbf{B}^{(0)} + O(\xi^2), \tag{B.11}$$

where $B_{nr}^{(0)} = \left[\lambda_n^{(0)}\right]^4$ for $n = r$ and $B_{nr}^{(0)} = 0$ for $n \neq r$.

The matrices on the left hand side of (27) can be approximated now as

$$\mathrm{Fr}^2\xi^2\mathbf{C} - \beta\mathbf{B} + (\alpha\mathrm{Fr}^2\xi^2 - 1)\mathbf{I} = \mathrm{Fr}^2\mathbf{C}^{(0)} - \beta\mathbf{B}^{(0)} - \mathbf{I} + O(\xi^2) = \mathbf{T}^{(0)} + O(\xi^2), \tag{B.12}$$

$$\beta\xi\tau\mathrm{Fr}\mathbf{B} = \beta\tau\mathrm{Fr}\left[\xi\mathbf{B}^{(0)} + O(\xi^3)\right]. \tag{B.13}$$

Up to the order $O(\xi^2)$ as $\xi \to 0$, equations (27) read as

$$\begin{cases} \mathbf{T}^{(0)}\vec{F}^R - \beta\xi\tau\mathrm{Fr}\mathbf{B}^{(0)}\vec{F}^I = \vec{P}(\xi) + O(\xi^2), \\ \beta\xi\tau\mathrm{Fr}\mathbf{B}^{(0)}\vec{F}^R + \mathbf{T}^{(0)}\vec{F}^I = O(\xi^3). \end{cases} \tag{B.14}$$

Equations (2), (16) and (25) show that $\vec{P}(\xi) = \vec{P}^{(0)} + O(\xi^2)$ as $\xi \to 0$. Then the solution of (B.14) is $\vec{F}^R = \vec{F}^{(R,0)} + O(\xi^2)$ and $\vec{F}^I = \xi\vec{F}^{(I,0)} + O(\xi^3)$, where

$$\mathbf{T}^{(0)}\vec{F}^{(R,0)} = \vec{P}^{(0)}, \tag{B.15}$$

$$\beta\tau\mathrm{Fr}\mathbf{B}^{(0)}\vec{F}^{(R,0)} + \mathbf{T}^{(0)}\vec{F}^{(I,0)} = 0. \tag{B.16}$$

Finally, we obtain

$$\vec{F}^{(R,0)} = \left[\mathbf{T}^{(0)}\right]^{-1}\vec{P}^{(0)}, \tag{B.17}$$

$$\vec{F}^{(I,0)} = -\beta\tau\mathrm{Fr}\left[\mathbf{T}^{(0)}\right]^{-1}\mathbf{B}^{(0)}\vec{F}^{(R,0)}. \tag{B.18}$$

More terms in the solution of (27) can be obtained as $\xi \to 0$. However, the formulae for the higher terms are complicated and not practical. It is easier to solve system (27) numerically for small positive values of ξ.

References

[1] V. A. Squire, R. J. Hosking, A. D. Kerr, P. J. Langhorne, Moving Loads on Ice Plates, Kluwer Academic Publishers, 1996.
[2] D. Y. Kheisin, Moving load on an elastic plate which floats on the surface of an ideal fluid (in russian), Ivz. AN SSSR, Otd, Tekh. i Mashinostroenie 1 (1963) 178–180.
[3] J. W. Davys, R. J. Hosking, A. D. Sneyd, Waves due to a steadily moving source on a floating ice plate, Journal of Fluid Mechanics 158 (1985) 269–287.
[4] E. I. Parau, F. Dias, Nonlinear effects in the response of a floating ice plate to a moving load, Journal of Fluid Mechanics 460 (2002) 281–305.
[5] F. Bonnefoy, M. H. Meylan, P. Ferrant, Nonlinear higher-order spectral solution for a two-dimensional moving load on ice, Journal of Fluid Mechanics 621 (2009) 215–242.
[6] E. Dinvay, H. Kalisch, P. E. I., Fully dispersive models for moving loads on ice sheets, Journal of Fluid Mechanics 876 (2019) 122–149.
[7] R. J. Hosking, A. D. Sneyd, D. W. Waugh, Viscoelastic response of a floating ice plate to a steadily moving load, Journal of Fluid Mechanics 196 (1988) 409–430.
[8] V. M. Kozin, A. V. Pogorelova, Effect of the viscosity properties of ice on the deflection of an ice sheet subjected to a moving load, Journal of Applied Mechanics and Technical Physics 50 (2009) 484–492.
[9] E. I. Parau, J. M. Vanden-Broeck, Three-dimensional waves beneath an ice sheet due to a steadily moving pressure, Philosophical Transactions 369 (2011) 2973–2988.
[10] T. Tabata, Studies on visco-elastic properties of sea ice, Arctic Sea Ice 598 US National Academy of Sciences and National Research Council (1958) 139–147.
[11] T. Takizawa, Deflection of a floating sea ice sheet induced by a moving load, Cold Regions Science and Technology 11 (1985) 171–180.
[12] D. V. Evans, R. Porter, Wave scattering by narrow cracks in ice sheets floating on water of finite depth, Journal of Fluid Mechanics 484 (2003) 143–165.
[13] R. Porter, D. V. Evans, Diffraction of flexural waves by finite straight cracks in an elastic sheet over water, Journal of Fluids Structures 23 (2007) 309–327.
[14] Z. F. Li, G. X. Wu, K. Ren, Wave diffraction by multiple arbitrary shaped cracks in an infinitely extended ice sheet of finite water depth, Journal of Fluid Mechanics 893 (2020) A14.
[15] T. D. Williams, R. Porter, The effect of submergence on the scattering by the interface between two semi-infinite sheets, Journal of Fluids and Structures 25 (2009) 777–793.
[16] L. A. Tkacheva, Wave motion in an ice sheet with crack under uniformly moving load, Fluid Dynamics 54 (2019) 14–32.
[17] Y. Z. Xue, L. D. Zeng, B. Y. Ni, A. A. Korobkin, T. I. Khabakhpasheva, Hydroelastic response of an ice sheet with a lead to a moving load, Physics of Fluids 33 (2021) 037109.
[18] A. A. Korobkin, T. I. Khabakhpasheva, A. A. Papin, Waves propagating along a channel with ice cover, European Journal of Mechanics-B/Fluids. 47 (2014) 166–175.
[19] E. A. Batyaev, T. I. Khabakhpasheva, Hydroelastic waves in a channel covered with a free ice sheet, Fluid Dynamics. 50 (2015) 775–788.
[20] K. Ren, G. X. Wu, Z. F. Li, Hydroelastic waves propagating in an ice-covered channel, Journal of Fluid Mechanics 886 (2020) 1–24.
[21] K. Shishmarev, T. I. Khabakhpasheva, A. A. Korobkin, The response of ice cover to a load moving along a frozen channel, Applied Ocean Research 59 (2016) 313–326.
[22] T. I. Khabakhpasheva, K. Shishmarev, A. A. Korobkin, Large-time response of ice cover to a load moving along a frozen channel, Applied Ocean Research 86 (2019) 154–165.
[23] G. E. Mase, Theory and Problems of Continuum Mechanics, volume 970, McGraw-Hill New York, 1970.

[24] S. P. Timoshenko, S. Woinowsky-Krieger, Theory of plates and shells, McGraw-hill, 1959.
[25] P. Brocklehurst, A. Korobkin, E. I. Parau, Hydroelastic wave diffraction by a vertical cylinder, Philosophical Transactions of the Royal Society A: Mathematical, physical and engineering sciences 369 (2011) 2832–2851.
[26] L. D. Zeng, A. A. Korobkin, B. Y. Ni, Y. Z. Xue, Flexural-gravity waves in ice channel with a lead, Journal of Fluid Mechanics 921 (2021).
[27] L. D. Zeng, A. A. Korobkin, B. Y. Ni, Y. Z. Xue, Hydroelastic waves propagating in a shallow fluid contained in a channel covered by two ice sheets of finite width, 25th IAHR International Syposium on Ice (2020).
[28] E. Kausel, J. Estaire, I. Crespo-Chacn, Proof of critical speed of high-speed rail underlain by stratified media, Proceedings of The Royal Society A 476 (2020) 20200083.